

Accurate 3D object profiling by FMCW optical ranging system using a VCSEL

メタデータ	言語: eng 出版者: 公開日: 2020-10-30 キーワード (Ja): キーワード (En): 作成者: メールアドレス: 所属:
URL	http://hdl.handle.net/2297/00059757

This work is licensed under a Creative Commons Attribution-NonCommercial-ShareAlike 3.0 International License.



Dissertation

ACCURATE 3D OBJECT PROFILING BY FREQUENCY MODULATION CONTINUOUS WAVE (FMCW) OPTICAL RANGING SYSTEM USING A VCSEL

***VCSEL を用いた FMCW 光距離センサによる精密 3D 物体
形状計測)***

**Graduate School of
Natural Science & Technology
Kanazawa University**

Division of Electrical Engineering and Computer Science

**Student ID Number : 1724042005
Name : Rini Khamimatul Ula
Chief Supervisor : Prof. Koichi Iiyama
Date of Submission : January 2020**

TABLE OF CONTENTS

LIST OF FIGURES	iii
LIST OF TABLE	vi
ABSTRACT.....	vii
ACKNOWLEDGMENTS	viii
Chapter 1 Introduction.....	1
1.1 Overview.....	1
1.2 Research Gap	2
1.3 Thesis Objectives	2
1.4 Motivation and Previous Research	3
1.5 Thesis Outline	4
Chapter 2 Basic of FMCW Optical Ranging System Using VCSEL	5
2.1 Introduction FMCW Reflectometry.....	5
2.2 Vertical Cavity Surface Emitting Lasers (VCSEL).....	9
2.3 Distributed Feedback Laser (DFB) Lasers Diode.....	10
2.4 Spatial Resolution and Ranging Accuracy	11
2.5 The Type of Interferometer.....	12
2.6 Fast Fourier Transform	14
Chapter 3 System Configuration.....	15
3.1 Experimental setup.....	15
3.2 Two-Dimensional Galvano Scanner	17
Chapter 4 Result and Analysis.....	18
4.1 Spatial Resolution and Ranging Accuracy	18
4.2 Object Profiling.....	23
4.3 Short Measurement Time Object Profiling	25
4.3.1 Without optimizing timing method.....	25
4.3.2 With optimizing timing method.....	28
4.4 Symmetric and Asymmetric Method	31
4.4.1 Symmetric Method.....	31
4.4.2 Asymmetric Method	34

4.5 Filtering.....	37
Chapter 5 Summary	40
References.....	41
APPENDIX.....	47

LIST OF FIGURES

Figure 2.1	The classification of optical ranging system.	5
Figure 2.2	The basic configuration of the FMCW optical ranging system.	6
Figure 2.3	Waveform of the optical frequency change of the reference and the reflected lights.....	7
Figure 2.4	The concept of VCSEL [29].....	9
Figure 2.5	Schematic drawing of the DFB laser [45].	11
Figure 2.6	Schematic beat spectrum and definition of the spatial resolution.	12
Figure 2.7	The Michelson interferometer [50].	13
Figure 2.8	The Mach-Zehnder Interferometer [54].	13
Figure 3.1	The experimental setup of FMCW optical ranging system for object profiling. (FC1, FC2, FC3: Fiber couplers, Cir: Circulator, PD: Photodiode)	15
Figure 3.2	Schematic of the propagation of the laser light after reflected by a one-dimensional Galvano mirror.....	17
Figure 4.1	Result of measured frequency modulation (FM) efficiency of the VCSEL and the DFB laser.	18
Figure 4.2	Whole beat spectrum.	19
Figure 4.3	Enlarge beat spectrum around the peak.....	20
Figure 4.4	Parabolic fitting to obtain the exact distance.....	20
Figure 4.5	Histogram of the measured distance error for 10000-times measurements at a distance of 17 cm.	21
Figure 4.6	Relationship between the FWHM and the standard deviation.	22
Figure 4.7	Measured displacement against the small displacement.	22
Figure 4.8	Three-dimensional profiling result of a Japanese 100YEN coin.....	23
Figure 4.9	Two-dimensional profiling result around the center of a Japanese 100YEN coin.	24

Figure 4.10 Photograph and three-dimensional profiling result of a printed circuit board.	25
Figure 4.11 Timing without optimizing timing method.	25
Figure 4.12 Three-dimensional profiling result of a Japanese 100YEN coin without optimizing timing for $f_m = 1$ kHz.....	26
Figure 4.13 Step response of the Galvano mirror.	27
Figure 4.14 Three-dimensional profiling result of a Japanese 100YEN coin using without optimizing timing method and the VCSEL as the laser source.	27
Figure 4.15 Timing with optimizing timing method.	28
Figure 4.16 Three-dimensional profiling result of a Japanese 100YEN coin with reduced number of acquired data for $f_m = 1.5$ kHz.	28
Figure 4.17 Three-dimensional profiling result of a Japanese 100YEN coin with different number of acquired data for $f_m = 1.8$ kHz.	29
Figure 4.18 Three-dimensional profiling result of a Japanese 100YEN coin with different number of acquired data for $f_m = 2.0$ kHz.	31
Figure 4.19 Analysis of data signal using the symmetric method	32
Figure 4.20 Three-dimensional profiling result of a Japanese 100YEN coin using the symmetric method with a different repetition frequency of the injection current modulation.	33
Figure 4.21 Relationship between the repetition frequency of the injection current modulation and the measurement time.	34
Figure 4.22 Timing of the data acquisition and the FFT analysis for the asymmetric method.	35
Figure 4.23 Three-dimensional profiling result of a Japanese 100YEN coin using the asymmetric method with $f_m = 1.0$ kHz, $T_r = 620$ μ s, $T_f = 380$ μ s and the number of acquired data is 1650 points.	35
Figure 4.24 Three-dimensional profiling result of a Japanese 100YEN coin using the asymmetric method with different f_m and periods in the increasing and the decreasing sections.....	36

Figure 4.25 Three-dimensional profiling result of a Japanese 100YEN coin after different types of filtering with $f_m = 1.8$ kHz and the number of acquired data is 600 points.
.....38

Figure 4.26 Three dimensional profiling result of a Japanese 100 YEN coin (a) without filtering (b) by 3-points median filter for x -direction and (c) by 3 x 3 median filter.
.....39

LIST OF TABLE

Table 4-1 Operating Condition of the DFB laser and the VCSEL. 19

ABSTRACT

In electronic and automotive device, the accuracy size and the precise shape of the component is the essential aspects to determine the quality of the product. Nowadays, an inspection on the shape of the mechanical electronics component in the automotive and electronic industry still using the human eye and camera that need long measurement time. That industry needs the sensing system that capable of inspecting the object, profiling a small object without contacting and harming, generate the clear object profiling with high spatial resolution and high ranging accuracy in the short measurement time. The Frequency modulation continuous waves (FMCW) reflectometry is the one of reflectometry type that very suitable to be applied in the systems that require the combination between of high speed, sensitivity and high resolution in the medium long-range. We developed the proposed sensing system based on FMCW optical ranging system using the VCSEL to generate clear object profiling with high spatial resolution, the high standard deviation in the short measurement time. In this study, we compare the VCSEL and the DFB laser diode as the laser source and the experiment result shows that VCSEL has the spatial resolution and standard deviation better than the DFB laser diode, because VCSEL has the wide optical frequency sweep range. The experimental spatial resolution defined by the FWHM is $460\ \mu\text{m}$ and the standard deviation of the measurement error is $2.7\ \mu\text{m}$. We were successful in profiled the three-dimensional of a Japanese 100YEN coin and a printed circuit. The short measurement time was achieved by increasing the repetition frequency of the injection current modulation and optimizing the timing of the data acquisition, the Galvano mirror scan and the FFT analysis by taking account of the transient response of the Galvano mirror. The fastest measurement time for profiling a coin with the resultant profiled data of 201×201 points is 22.6 sec. Improving the quality of object profiling by 3-points median filter for x -direction. The median filter is effective to eliminate spike noise. The developed system is very useful for industrial application such as diagnostic the shape of components in automotive and electronic industries, and profiling of mechanical workpieces and inspection in the mechanical and electrical assembly process.

ACKNOWLEDGMENTS

Praise me for the presence of Allah SWT who has guided, helped and provided convenience in my research and studies so that I could complete this dissertation as a graduation requirement as a doctorate in Kanazawa University

I would like to offer my deepest gratitude to my best supervisor, Prof. Koichi Iiyama. Thank you very much for the opportunity for choosing me as a doctoral student at Optical and Electrical Sensing Laboratory (Oeslab), the patience guiding during my study and research, the extraordinary help in preparing my paper and our lives while staying in Japan and the best advice for my research and education. I also would like my sincere gratitude to my co-advisor, Assoc. Prof. Takeo Maruyama for his deep involvement. Thanks a lot to all Oeslab member for their advice and support help during the experimental works.

I would like to express my most profound appreciation for my beloved parents, Bapak Mu'alimin and Ibu Nurhayati whose always duaa and give the best support for everything. This dissertation presents to my husband and my two beloved daughters, Najwa and Tazkiyah who have always been my motivation in studying and working. Thanks are also to my big Family for supports and help in everything.

Chapter 1

Introduction

1.1 Overview

The accurate size and the precise shape of components in electronic and automotive device are the critical aspects to determine the quality of the product. The inaccuracy of the element will influence the performance of the product and even causes an accident. Nowadays, an inspection of the accuracy of the location and shape of mechanical electronics components in the automotive and electronic industry are still using human eyes and cameras. This method requires long measurement time for the inspection and has possibility of human error. Since the industry needs the sensing system that is capable for inspecting the object and profiling small objects without contacting and harming, a high-speed ranging system with high spatial resolution and high ranging accuracy is required.

In a long time ago, the practical application of fiber optic sensor techniques has developed from the experimental stage. Optical sensing is a promising sensing system having many advantages, i.e. non-contact sensing, high ranging accuracy, high resolution, non-interference by electromagnetic waves, high measurement accuracy, extremely optical low-cost, low-power consumption, and easily be interfaced with the data communication system [1][2][3]. The decreasing price for commercial components for optical sensing results in increased number of researchers developing and studying optical sensing. In parallel with this development, the quality improvements of optical sensing have been made, and many conventional sensors were replaced by optical sensors [4].

Since a few decades, the reflectometric techniques (reflectometry) were established for nondestructively diagnosing fiber-optic devices [5]. The proposed sensing system will be used for diagnosing and profiling of objects in short and medium range. The Frequency modulated continuous waves (FMCW) reflectometry is one of the reflectometry that is very suitable to be applied in the systems that require the combination between of high speed, sensitivity and high resolution in the medium long-range [6].

FMCW reflectometry is also known as the coherent optical frequency domain reflectometry (OFDR) and have been studied and developed by many researchers. Tunable laser-based OFDR was developed and was shown to be effective for lengths over 200 m with

the resolution of about 100 μm [7]. A low-cost self-heating sweep VCSEL based OCT system was successfully developed to provide the axial resolution of 135 μm in air, the sensitivity of -91 dB, and was shown to be capable as economical alternative for long-range applications of OCT [8]. The FMCW optical sensing system with symmetric triangular signal for the optical frequency sweep of a laser source was successfully developed and applied to three-dimensional object profiling of a Japanese 100YEN coin with the resultant profiled data of 201 x 201 points, the measurement time of 84 sec, and the spatial resolution of 0.9 mm by using a VCSEL as the laser source [9][10][6][11][12].

Based on that phenomenon and demands in industry and research, we here focus on the development of the sensing system based on the FMCW optical ranging system using a VCSEL to generate accurate 3D object profiling in the short measurement with high spatial resolution and ranging accuracy. Because of that, we choose the title “Accurate 3D Object Profiling by FMCW Optical Ranging System using a VCSEL” as a topic in our research.

1.2 Research Gap

Diagnosing the shape of the component in the electronic and automotive industry using the human skill widely results in slight imperfectness of product caused by the low measurement accuracy. Besides that, using the human skill and camera as quality control of the shape component requires in the long measurement time for about 2 – 3 minutes.

The low measurement accuracy of profiling the component causes the product be low quality and low safety. Long measurement time for diagnosing the component results in high production cost because of low production speed due to limited diagnosing speed of human.

1.3 Thesis Objectives

The FMCW reflectometry is widely used for radar to measurement distance to the object in long-range. However, to overcome the issues mentioned above, in this study, we developed the optical sensing system based on the FMCW optical ranging system using a VCSEL as a laser source. The purposes of this study are as follows:

1. To realize the optical sensing system that capable of generating clear object profiling
2. To achieve the short measurement time for clear object profiling

3. To achieve the high spatial resolution
4. To achieve the high ranging accuracy.

1.4 Motivation and Previous Research

High-speed measurement to diagnose an object and capable of producing high quality and high safety product is the motivation to develop the optical sensing system with the characteristics such as capable of generating clear object profiling in the short measurement time and high spatial resolution and ranging accuracy.

In the previous study, many researchers have studied and developed optical sensing system based on the reflectometry, especially FMCW reflectometry.

- Brian J. Soller *et al.* (2005) has developed the tunable laser-based OFDR and showed the effectiveness for long-range measurement over 200 m with the resolution for about 100 μm [6].
- Yongwoo Park *et al.* (2007) shows unique reflectometry named chirped fiber Bragg grating OFDR based on real-time Fourier transformation (LCFG-based OFDR-RTFT). The OFDR is potentially attractive for imaging applications that require high sensitivities, long depth range, high resolution and ultrahigh acquisition speed.
- Tatsuo Hariyama *et al.* (2018) configures a low-cost 3D imaging system using a directly modulated VCSEL as FMCW source with 10-cubic-meter imaging volume with the resolution and accuracy are 0.36 mm and 5.7 μm , respectively [13].
- Koichi Iiyama *et al.* (2016) demonstrates the FMCW optical sensing system using a VCSEL as the laser source, and was succeeds to three-dimensional object profiling of a Japanese 100YEN coin with the profiled data of 201 x 201 points, the measurement time of 84 sec, and the spatial resolution of 0.9 mm [13][14][15][9].

In this study, we will improve the FMCW optical ranging system using a VCSEL as a laser source to generate the clear three-dimensional object profiling with the measurement time of about 20 sec, high spatial resolution and high ranging accuracy.

1.5 Thesis Outline

This thesis is divided into five-chapter. Chapter 1 is the overview and the explanation of the research background based on the problem in the electronics and automotive industry that human skill and cameras are now used to diagnostic the shape of components, and the research purpose is also explained. The goal of this research is to achieve clear object profiling with high spatial resolution, high ranging accuracy in the short measurement time. The research gap and the motivation of this research are explained in this chapter together with the previous study.

Chapter 2 consists of the introduction of the frequency modulation continuous wave (FMCW) reflectometry and its advantages. The operating principles of laser sources used in the experiments, the vertical-cavity surface-emitting laser (VCSEL) and the distributed feedback (DFB) laser, are explained in this chapter. In the experimental setup of the FMCW optical ranging system, two types of interferometers, the Michelson interferometer and the Mach-Zehnder interferometer, are used, and the principle of the interferometers are explained. The sensing signal is analyzed by the FFT to estimate the distance, and the resultant spatial resolution is also explained.

The experimental setup and the method of this research are explained in Chapter 3. Chapter 4 presents the experimental results, and shows the spatial resolution of the optical ranging system of $2.3\ \mu\text{m}$ and the spatial resolution of $2.7\ \mu\text{m}$ when using a VCSEL as the frequency-swept laser source. We also show that the developed sensing system is useful of not only the three-dimension of object profiling but also measurement the thickness of an object. The short measurement time is achieved when using optimizing timing of the data acquisition and the signal analysis, and the object profiling become clearer by using a 3-points median filter for x-direction.

Chapter 2

Basic of FMCW Optical Ranging System Using VCSEL

2.1 Introduction FMCW Reflectometry

Optical reflectometry is very suitable for diagnosing optical fibers without harming [16]. Since this method has an insufficient spatial resolution, it cannot be applied for characterizing integrated optical devices. The optical reflectometry is a critical investigation system for light-wave systems and components. Based on the measurement range and the spatial resolution, the ranging optical system or optical reflectometry is classified into three types as shown in Fig. 2.1 [17], [18], based on the basic physics, spatial resolution, measurement speed, sensitivity, and accuracy [17]–[22]:

1. Time of flight (ToF) illuminates modulated light (pulse or sinusoidally modulated) and then measured the delay time or the phase delay of the returning light from an object [23]. The ToF is applicable to measure the distance in the range of 10 cm ~ more than 100 m with the spatial resolution of 1 cm ~ 10 cm. The most popular application for the ToF in optical imaging is the 3D camera in the long-range measurement.
2. The frequency modulation continuous wave (FMCW) sensing system has the measurement range of 1 cm ~ more than 10 m. The FMCW sensing system requires a high coherent single-mode laser.

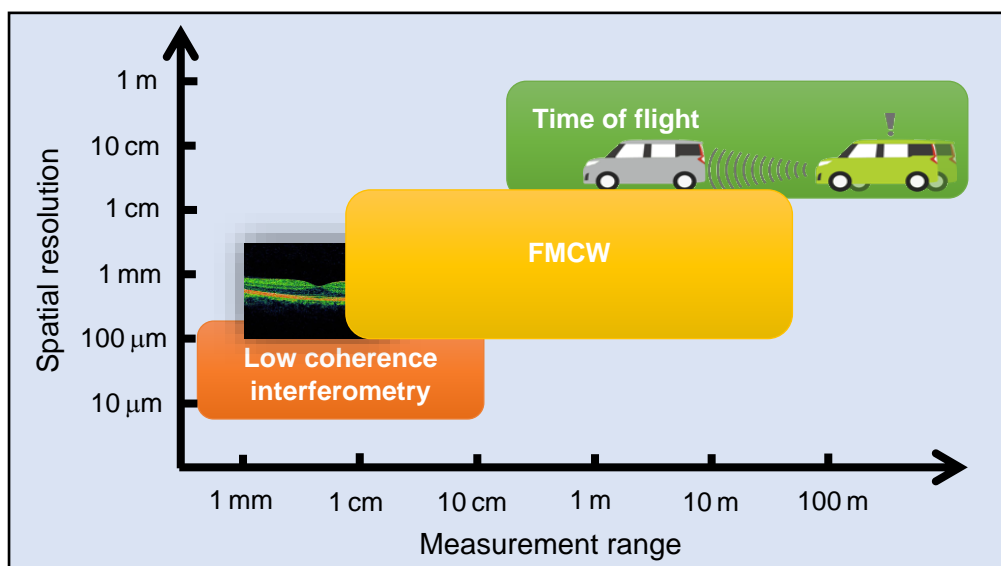


Figure 2.1 The classification of optical ranging system.

3. The low coherent interferometry measures the interference signal between the reflected light on an object and a reference light under broadband light illumination. Although the measurement range is limited to be less than 10 cm, the spatial resolution is as high as $10\ \mu\text{m} \sim 100\ \mu\text{m}$. The typical application of the low coherence interferometry is medical application such as diagnosing human eyes.

The frequency modulation continuous wave (FMCW) optical ranging system is a high-resolution ranging system using an optical frequency-swept laser source. The FMCW optical ranging system has been studied as the FMCW reflectometry and is known as optical frequency domain reflectometry (OFDR). The OFDR can be divided into two categories: the incoherent OFDR (I-OFDR) and the coherent OFDR (C-OFDR)[16]. The I-OFDR is widely used to the characterization of optical devices and fiber lines [24]. In this method, the continuous wave of the probe signal is modulated by a constant amplitude RF signal [25], and the frequency is linearly swept. The probe signal and the modulating RF signal is mixed in the electrical domain [25] and then the spectrum is observed using an electrical spectrum analyzer [25].

In the C-OFDR or also known as the FMCW reflectometry, the optical frequency of the laser source is linearly swept in time. As shown in Fig. 2.2, the basic configuration of the FMCW optical ranging system consists of an optical frequency-swept laser source, a two-beam interferometer and a target that located in an arm of the interferometer. The laser beam is divided into two-beam i.e. reference beam and reflected beam. The reference beam is propagated directly to the photodetector, and the reflected beam enters to the target. The reflected light from the target interferes with the reference light in the photodetector (PD) [1], [6]. The coherent length of the light source limits the measurement range of the FMCW optical ranging system [26]. The measurement range can be extended by using the laser source that has a narrow-linewidth [26].

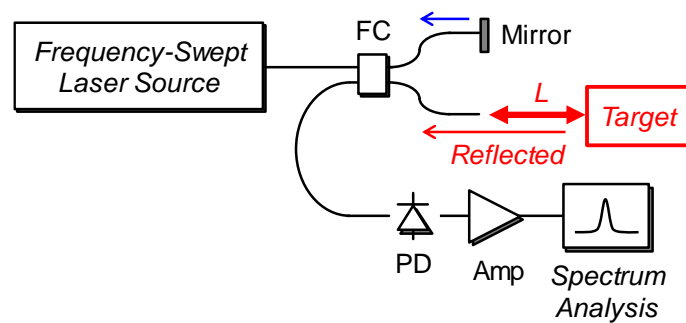


Figure 2.2 The basic configuration of the FMCW optical ranging system.

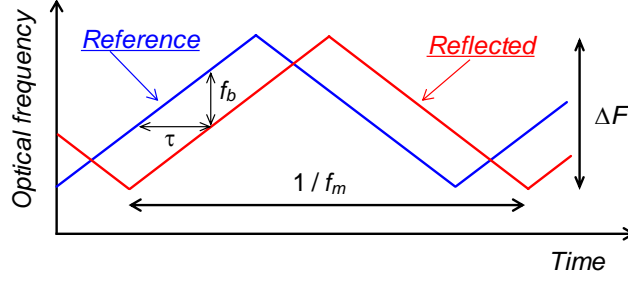


Figure 2.3 Waveform of the optical frequency change of the reference and the reflected lights.

Figure 2.3 shows the waveform of the reference and the reflected lights. The optical frequency is symmetrically linearly swept in time. The interference signal in the increasing section or the decreasing section of the optical frequency sweep is measured to prevent the phase discontinuity in the interference signal at the turning points of the optical frequency sweep.

As is shown in Fig. 2.3, there is a propagation delay time τ between the reference light and reflected light, and the propagation delay time is given by [6]:

$$\tau = \frac{2nL}{c} \quad (1)$$

where

n : the refractive index of the optical fiber

L : the differential distance between the reference and reflected lights

c : the light velocity in vacuum.

If the symmetric triangular waveform is used for sweeping the optical frequency of laser source, the beat frequency of the interference signal, which is the optical frequency difference between the reference light and the reflected light, is given by:

$$f_b = 2f_m \Delta F \times \tau \quad (2)$$

By substituting eq. (1) into eq. (2), the beat frequency is given by:

$$f_b = \frac{4nf_m \Delta F}{c} L = \frac{2n}{c} \gamma L \quad (3)$$

with

$$\gamma = 2f_m \Delta F \quad (4)$$

where

f_m : the repetition frequency of the optical frequency sweep

ΔF : the optical frequency sweep range

γ : the optical frequency chirp rate.

Equation (3) declares that the beat frequency in the interference signal is proportional to the distance L , and then the distance is obtained by measuring the beat frequency by Fourier analysis of the interference signal.

As described above, the interference signal in the increasing section or the decreasing section of the optical frequency sweep is measured and the beat spectrum is obtained by FFT analysis for the measured data. Since the measured time is half of the period of the optical frequency sweep, which is given as $1/(2f_m)$, the beat spectrum is given as sinc function. The spatial resolution defined by the Rayleigh resolution of the beat spectrum is given as:

$$\delta L = \frac{c}{2n\Delta F}. \quad (5)$$

The spatial resolution can be enhanced increasing the optical frequency sweep range ΔF [26]. The FMCW reflectometry is very suitable for the applications that require the combination between high speed, high sensitivity and high resolution in the medium measurement range [24] [27].

The Rayleigh scattering is the high-intensity elastic scattering of light based on density and random compositional fluctuation of fiber materials and suitable for used in fiber integrity sensing and interferometric sensing.

In optical reflectometry application, high spatial resolution is desired to distinguish adjacent fault location. Beside the object profiling, the other implementation of the FMCW optical ranging system is characterization and diagnosis of fault locations in optical fibers and optical waveguide devices and optical coherent tomography (OCT) for imaging human eye and fingertip. For imaging human eye and fingertip application, high spatial resolution of about 10 μm and the measurement range of about 1 cm is required. For object profiling application, the measurement range should be longer than imaging application of human imaging eye and fingertip.

2.2 Vertical Cavity Surface Emitting Lasers (VCSEL)

In 1977, Prof. K. Iga at Tokyo Institute of Technology proposed the concept of the vertical-cavity laser source [28]. The cavity of the VCSEL is the vertical shape and consists of mirrors on the top and the bottom of the active layer as in Fig. 2.4. The mirrors have very high reflectivity by distributed Bragg reflector (DBR) mirrors formed by multilayer quarter-wavelength dielectric stack. To reach the threshold in very short cavity, multi quantum well (MQW) structure is employed in the active layer [29]. The light is reflected in vertical direction through the active region by the two DBR mirrors.

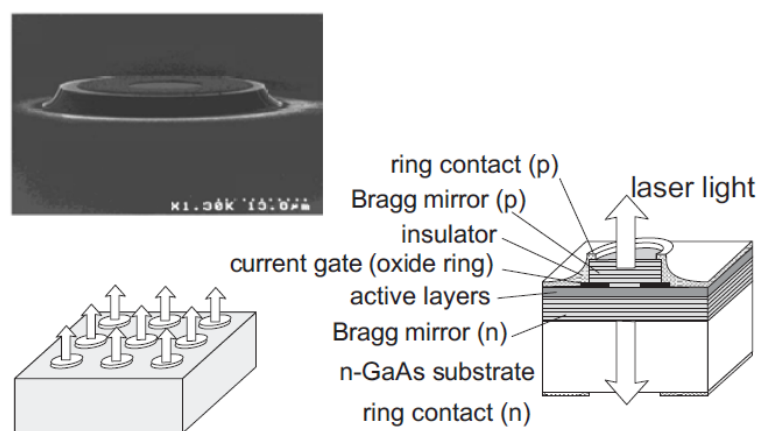


Figure 2.4 The concept of VCSEL [29].

The VCSEL is eligible as the laser source because has many advantages as follows; [8], [13], [14], [28], [30]–[40]:

- low-cost data transmission,
- possibility of high-frequency direct modulation in the range of multi gigahertz,
- inexpensive mounting technology and high coupling efficiency to lens and optical fibers because the light of the VCSEL is emitted directly from the surface,
- the VCSEL has superior performance such as smaller size and lower energy consumption [41],
- low threshold current,
- single longitudinal mode operation,
- circular-output beam profile
- wafer-scale integrality.

Based on the several advantages described above, the VCSEL is highly recommended for optical communication and other applications. The VCSEL is usually used in 3D sensing applications for facial recognition in smartphones and high-bandwidth optical interconnections.

The polarization of the transverse mode of the VCSEL is not fixed because the VCSEL is normally has a symmetric structure. The VCSEL is usually operated in one linearly polarized fundamental transverse mode if it is used in the near-threshold current [42].

2.3 Distributed Feedback Laser (DFB) Lasers Diode

A distributed feedback (DFB) laser is a type of laser diodes, where the active region of the device contains a periodically structured element or diffraction grating [38]. The structure builds a one-dimensional interference grating (Bragg scattering) [36], [43]–[45] and the grating provides optical feedback for lasing. The optical feedback in the laser cavity is caused by the longitudinal diffraction grating that has periodic changes of the thickness of the laser cavity, which results in the periodic change of the effective refractive index. The grating and the resultant optical feedback in the DFB lasers are generally continuous along the cavity, instead of just being at the two ends. The DFB laser is used when clean single-mode operation is required, especially in high-speed fiber optic telecommunications [35], [36], [44]–[47]. The DFB lasers are more stable in the lasing wavelength compared to Fabry-Perot or DBR lasers.

Laser diodes have broad gain bandwidth. Hence a frequency-selective element is required in the laser cavity to obtain single wavelength in wide operation conditions. One of the frequency-selective elements is the Bragg reflector, which causes optical feedback for the wavelength satisfying the Bragg condition [48]. The grating in the distributed feedback (DFB) laser is formed in the gain region, and then a single frequency laser diode is obtained. The lasing property of DFB lasers depends on the properties of reflection [45]. If the grating is periodic and continuous and both the facets of the laser cavity are anti-reflection coated, there is no optical feedback other than the grating, then such a structure supports two longitudinal (degenerate) modes and almost always lases at two wavelengths. A quarter-wavelength phase shift in the grating is usually introduced to guarantee single-wavelength lasing.

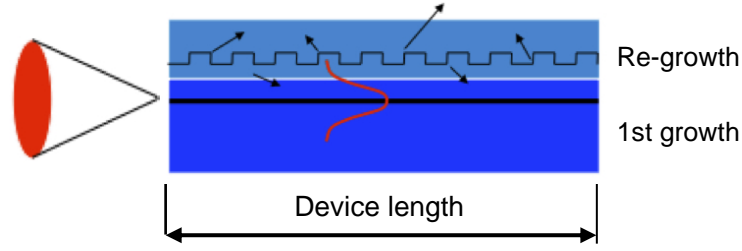


Figure 2.5 Schematic drawing of the DFB laser [45].

The DFB lasers and the distributed Bragg reflector (DBR) lasers have the same characteristics in the linewidth and wavelength tunability. The DFB lasers have a feedback structure consisting of low-contrast, weakly reflecting Bragg reflector distributed along the entire length of the gain ridge. Hence the name of the laser is the distributed feedback laser [36], [46], [49]. The DFB laser requires the grating to be buried under a high index layer, epitaxially regrown over the grating, to form the waveguide as shown in Fig 2.5.

2.4 Spatial Resolution and Ranging Accuracy

The spatial resolution is the minimum resolvable separation between adjacent reflecting points by the sensor. The image quality and details of object profiling can be determined by the spatial resolution. One of the advantages of the FMCW optical sensing system is high spatial resolution determined by the resolution of the beat spectrum [23]. Figure 2.6 shows the schematic beat spectrum using the Hanning window (in solid line) in the FFT and without using the window function (in the dashed line). The spatial resolution given in eq. (4) is defined as the differential distance between the peak and the first zero point in the $|\text{sinc}|$ function, which is the beat spectrum without using a window function in the FFT. In our experiments, the Hanning window was used. When using the Hanning window in the FFT, the first zero point cannot be clearly measured due to the reduced magnitude of the sidelobes, and then the spatial resolution is estimated by the full-width at half-maximum (FWHM) of the beat spectrum shown as the solid line in Fig. 2.6. The theoretical FWHM of the beat spectrum shown in Fig. 2.6 is given by

$$\delta L_{FWHM} = 2\delta L = \frac{c}{n\Delta F}. \quad (6)$$

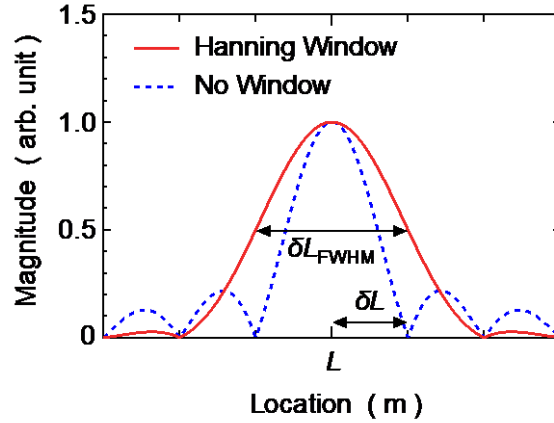


Figure 2.6 Schematic beat spectrum and definition of the spatial resolution.

2.5 The Type of Interferometer

Interferometric measurement requires two or more lights with different optical paths derived from a same laser source, and the lights interfere on a photodetector. Based on the number of interfering lights, the interferometer can be classified to two-beam interferometers and multiple-beam interferometers. The Michelson interferometer and the Mach-Zehnder interferometer are the best types of two-beam interferometers [51]. In our experiment, we used two two-beam interferometers, the sensing interferometer and the auxiliary interferometer. The sensing interferometer is the Michelson interferometer, and the auxiliary interferometer is the Mach-Zehnder interferometer.

The Michelson interferometer has been developed to investigate wave nature of light, and has also been used to provide evidence for the spectral theory of relativity [52] to detect and measure hyperfine structure in line spectra, to measure the tidal effect of the moon on the earth, and to provide a substitute standard for the meter in terms of wavelength of light [51].

The basic configuration of the Michelson interferometer shown in Fig. 2.7. In Fig 2.7, the refraction is ignored and anti-parallel lights are slightly displaced for the sake of clarity. Light from the source S is incident at 45° on a partial reflective surface M_3 of the beam splitter P_1 at point A. The transmitted light X passes through the phase compensator P_2 , is reflected back to point A through the phase compensator by reflection at the mirror M_1 , and then goes to the observer O. Meanwhile, the reflected light Y traverses P_1 , is reflected by the mirror M_2 , passes through P_1 , and recombines with light X as it goes to observer O. The phase compensator O2 ensures that both beams travel the same distance.

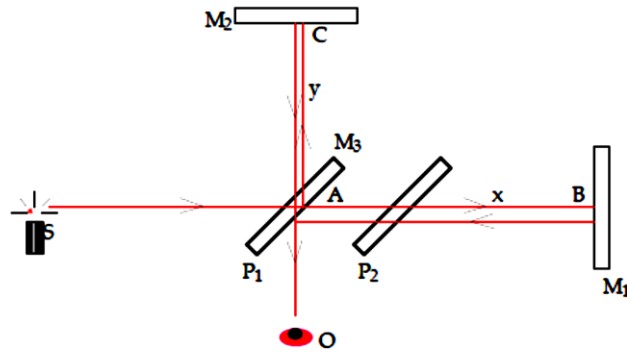


Figure 2.7 The Michelson interferometer [50].

The Michelson interferometer can be used to carry out the following principal measurement [52]:

- The width and fine structure of spectral line;
- Length or displacement in terms of the wavelength of light
- Refractive indices of transparent solids
- Differences in the velocity of light for different direction.

The Mach-Zehnder interferometer is basically used to measure the relative phase shift between two collimated lights from a coherent light source by changing the length of one of the arms or by placing a sample in path of one of the lights [53]. The optical devices used for optical signal processing such as switching, add-drop multiplexing, modulator and etc. has been developed using the Mach-Zehnder interferometer. The basic configuration of the Mach-Zehnder interferometer is shown in Fig. 2.8, where two-beam splitters and two mirrors are used to divide and recombine the lights [53].

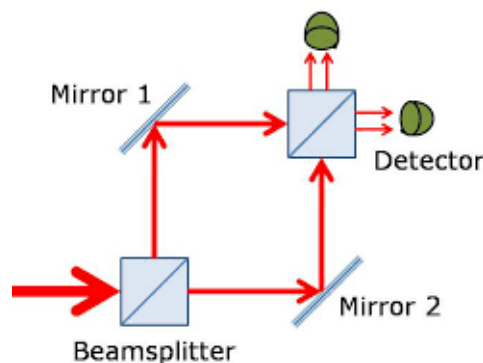


Figure 2.8 The Mach-Zehnder Interferometer [54].

2.6 Fast Fourier Transform

In 1965 Cooley and Tukey [57] were reported the fast Fourier transform (FFT) algorithm which requires much less computational effort. The FFT has significant effects in computational techniques in digital spectral analysis, filter, simulation, etc. For computational efficiency, the discrete Fourier transform (DFT) of a time series (discrete data samples) using the FFT is a recommended method. This method is more economical than in the previous methods because this method offers solutions to solve many problems [58].

The Fast Fourier Transform (FFT) and the power spectrum are powerful tools for analyzing and measuring signals from plug-in data acquisition (DAQ) devices [59], [60]. The time-domain signals are effectively acquired and the frequency content is easily achieved by using the FFT, which is an alternative to traditional benchtop spectrum and network analyzers. By using plug-in DAQ devices, the measurement system is lower cost and avoid the communication overhead of operating with stand-alone instruments. The basic functions for FFT-based signal analysis are the FFT and calculation of the power spectrum and the cross power spectrum [58]–[62]. Using these functions as building blocks, additional measurement functions such as the frequency response, the impulse response, the coherence, the amplitude spectrum, and the phase spectrum are easily realized. The FFT and the power spectrum are useful for measuring the frequency content of stationary or transient signals. The FFT produces the average frequency component of the acquired signal over the entire time.

The FFT is an algorithm that computes the DFT and the inverse DFT. A signal from its original domain (often times or space) is converted to the frequency domain and vice versa by Fourier analysis. The DFT is obtained by decomposing a sequence of values into components of different frequencies. This operation is useful in many fields, but computing it directly from the definition is often too slow and is not suitable for practical applications. The FFT rapidly computes such transformations by factorizing the DFT matrix into product of sparse (mostly zero) factors. There are many different FFT algorithms based on a wide range of published theories, from simple complex-number arithmetic to group theory and number theory. The FFT is widely used for applications in engineering, music, science, and mathematics.

Chapter 3

System Configuration

3.1 Experimental setup

Figure 3.1 shows the experimental setup of the FMCW optical ranging system, which is composed of the sensing interferometer and the auxiliary interferometer.

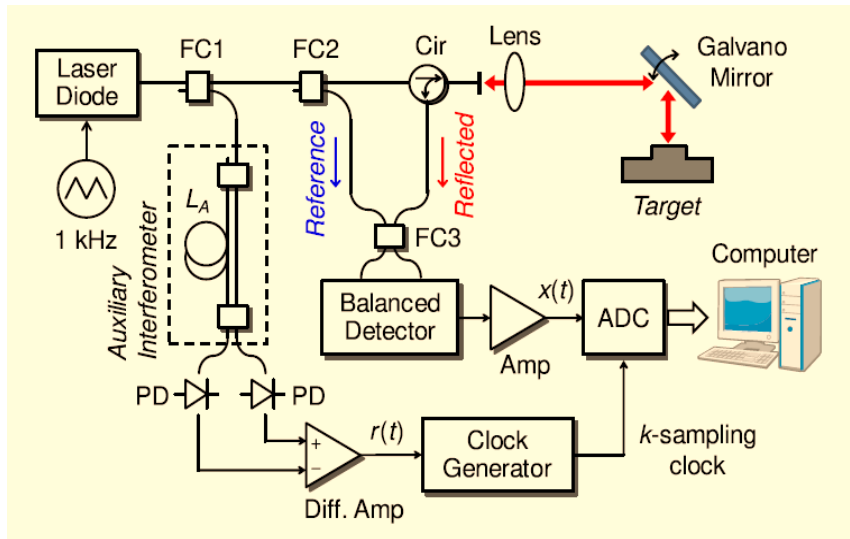


Figure 3.1 The experimental setup of FMCW optical ranging system for object profiling.

(FC1, FC2, FC3: Fiber couplers, Cir: Circulator, PD: Photodiode)

A laser diode emitting at 1310 nm is used as a light source and the optical frequency is swept by modulating the injection current with a symmetric triangular signal with the repetition frequency of 1 kHz. In the experiment, two types of laser diodes are used as the laser source, which are a DFB laser (Furukawa, FOL13F1MWS-A4-SA7) and a single-mode VCSEL (Raycan, RC22xxx1-T). The laser light is launched from the Circulator and the lens with the focal length of 20 cm. The laser light is propagated toward the Galvano mirror (Thorlabs, GVS002) used for scanning the laser light, and the scan area is wider than the target size. In the experiment, the beam size on the target is not measured, however is estimated to be a few tens μm by analysis from the profiling result. The reflected light from the target interferes with the reference light passed through the fiber couplers FC2 and FC3.

The beat spectrum will be spread out and the spatial resolution will be degraded if the optical frequency chirp rate γ , varies in time because the optical frequency sweep is nonlinear.

The optical frequency of the DFB laser and the VCSEL is changed by the injection current change. However the optical frequency change of the DFB laser and VCSEL lags behind the injection current [6][26]. Since the modulation frequency is as low as 1 kHz, the optical frequency of the DFB laser and the VCSEL is changed by thermal effect caused by the injection current change, the temperature change of the laser cavity cannot respond to the injection current change. As a result, the optical frequency of the DFB laser and the VCSEL is nonlinearly swept even though the injection current is modulation with a linear waveform such as a triangular signal.

The k -sampling technique is utilized in our system to cancel the influence of nonlinearity in the optical frequency sweep. As shown in Fig. 3.1, the k -sampling clock is generated from the interference signal of the auxiliary interferometer, $r(t)$ by using the clock generator, and the sensing interferometer signal, $x(t)$, is sampled with the k -sampling clock. The sampled sensing signal is used for analyzing the beat spectrum.

In the k -sampling technique, the Sampling theorem should be satisfied between the sensing interference signal $x(t)$ and the auxiliary interference signal $r(t)$. Then the measurement range L_{max} is given as [63]:

$$L_{max} = \frac{1}{4} n L_A \quad (7)$$

with

n : the refractive index of the optical fiber in the auxiliary interferometer

L_A : the length of the fiber delay line in the auxiliary interferometer,

where the different type of the interferometer, the Michelson interferometer type for the sensing interferometer and the Mach-Zehnder interferometer type for the auxiliary interferometer, is taking into account. When the beat frequency appears at the data point D in the beat spectrum, the distance L is given as:

$$L = \frac{D}{N/2} L_{max} = \frac{n L_A}{2N} D \quad (8)$$

where N is the number of data used in FFT analysis.

3.2 Two-Dimensional Galvano Scanner

In our experiment, we used the two-dimensional Galvano scanner for object profiling. The schematic of the propagation of the laser light after reflected by a one-dimensional Galvano mirror is shown in Fig. 3.2. The initial angle of the Galvano mirror is 45° and the laser light is normally illuminated onto the target as shown in Fig. 3.2(a). The distanced L_0 is measured by the FMCW optical ranging system. If the angle of the Galvano mirror is changed by θ_x with respect to 45° in the x -direction, the illuminating angle is changed by $2\theta_x$ as shown in Fig. 3.2(b), and the diagonal length to the target L is measured by the FMCW optical ranging system. Then the horizontal distance change x and the height z at the illuminated point are calculated as:

$$x = L \sin(2\theta_x) \quad (9)$$

$$z = L \cos(2\theta_x) \quad (10)$$

A two-dimensional Galvano mirror is used in our FMCW optical ranging system. If the angle of the Galvano mirror is changed by θ_x in the x -direction and θ_y in the y -direction, the horizontal distance change x , y and the hight z at the illuminated point are calculated from the measured diagonal length to the target L as:

$$x = L \sin(2\theta_x) \quad (11)$$

$$y = L \sin(2\theta_y) \quad (12)$$

$$z = L \cos(2\theta_x) \cos(2\theta_y). \quad (13)$$

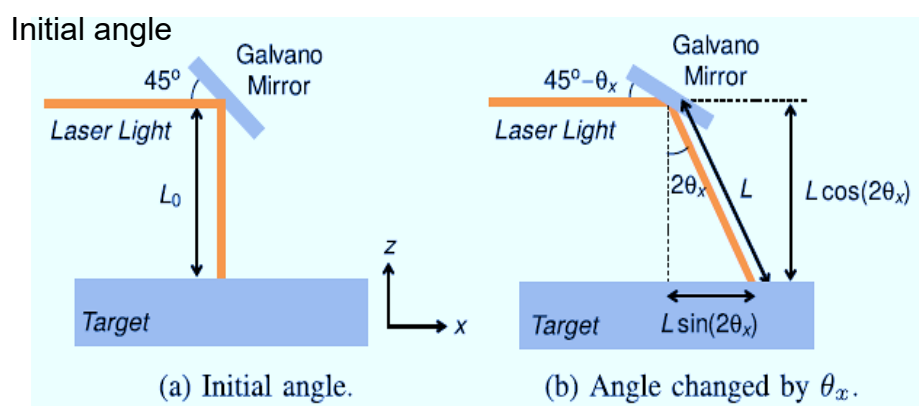


Figure 3.2 Schematic of the propagation of the laser light after reflected by a one-dimensional Galvano mirror.

Chapter 4

Result and Analysis

4.1 Spatial Resolution and Ranging Accuracy

At first, we measured the frequency modulation (FM) efficiency of the DFB laser and the VCSEL, and the result is shown in Fig. 4.1.

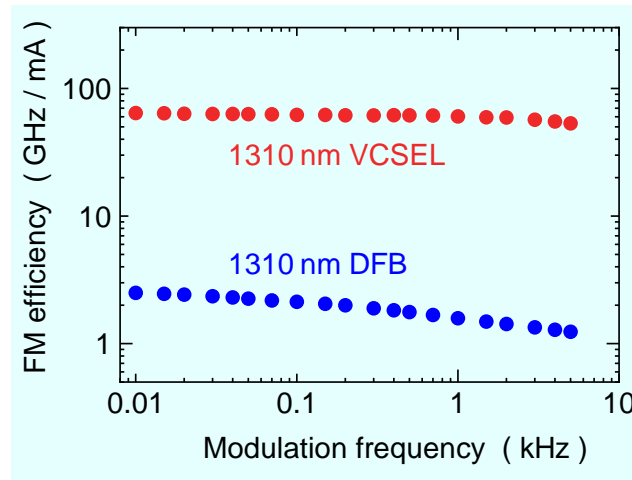


Figure 4.1 Result of measured frequency modulation (FM) efficiency of the VCSEL and the DFB laser.

When the VCSEL is used as the frequency-swept laser source at the modulation frequency is 1 kHz, the FM efficiency is 60 GHz/mA. By using the same the modulation frequency, the FM efficiency of the DFB laser is 1.6 GHz/mA. The FM efficiency of the VCSEL is 38 times higher than the DFB laser.

Table 4.1 shows the operation condition of the DFB laser and the VCSEL in our experiments. The DFB laser has the theoretical optical frequency sweep range of 136 GHz when the modulation amplitude is 100 mA_{p-p}, and the VCSEL has the theoretical optical frequency sweep range of 710 GHz when the modulation amplitude is 12 mA_{p-p}. From the values, the frequency modulation efficiency for the DFB laser is estimated to be 13.6 GHz/mA_{p-p} and 59 GHz/mA_{p-p} for the VCSEL. The above frequency modulation efficiency is slightly smaller than the result shown in Fig. 4.1 because the interference signal around the turning points of the modulation waveform is not used for the FFT analysis.

Table 4-1 Operating Condition of the DFB laser and the VCSEL.

Parameter	Notation	DFB	VCSEL
Threshold current	I_{th}	20 mA	1.2 mA
Maximum current	I_{max}	150 mA	15 mA
Bias current	I_{DC}	90 mA	8 mA
Modulation amplitude	ΔI	100 mA _{p-p}	12 mA _{p-p}
Optical frequency sweep range	ΔF	136 GHz	710 GHz
Theoretical spatial resolution	δL	1.10 mm	211 μm
Theoretical FWHM	δL_{FWHM}	2.20 mm	422 μm

In the previous chapter, the spatial resolution is defined as the full-width at half-maximum (FWHM) of the beat spectrum. In the research, the beat spectrum for a mirror located around 17 cm is measured and the FWHM is evaluated.

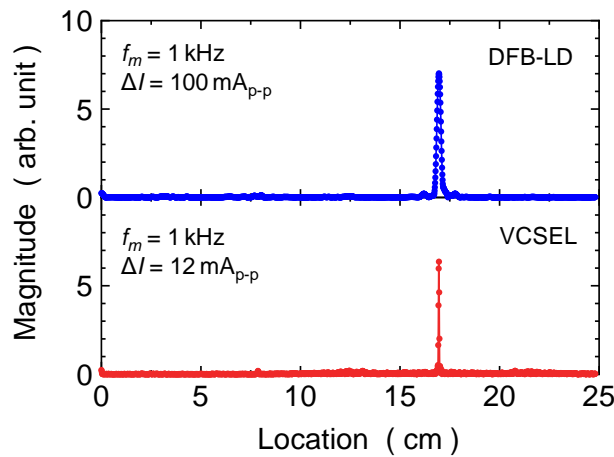


Figure 4.2 Whole beat spectrum.

The measured beat spectrum is shown in Fig. 4.2, where the upper is the beat spectrum when the DFB laser is used as the optical frequency-swept laser source, and the bottom is the beat spectrum when the VCSEL is used as the optical frequency-swept laser source. The beat spectrum using the VCSEL is narrower than the beat spectrum using the DFB laser.

Figure 4.3 is the enlarged beat spectrum around 17 cm to measure the FWHM. The FWHM is 2.3 mm when using the DFB laser and is 460 μm when using the VCSEL. The small value of the FWHM when using the VCSEL is due to the large optical frequency sweep range.

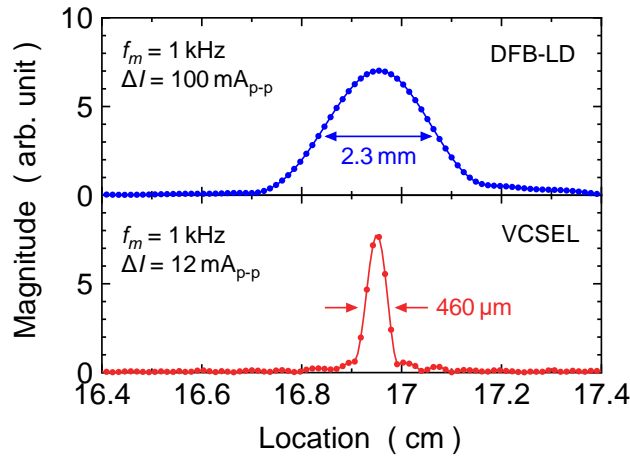


Figure 4.3 Enlarge beat spectrum around the peak.

The theoretical FWHM of the DFB laser and VCSEL is also available in Table 4.1. The measured FWHM is almost same with the theoretical FWHM in Table 4.1. From the result, the VCSEL is found to be a suitable laser source for optical ranging with high spatial resolution because the VCSEL has wider optical frequency sweep range ΔF .

Next we discuss the ranging precision. Since the beat spectrum is discrete, the exact distance cannot be obtained from the peak position of the beat spectrum. The exact distance evaluated by parabolic fitting around the peak in the spectrum as shown in Figure 4.4. The exact distance is estimated at the position where the magnitude of the fitted parabolic function is maximum.

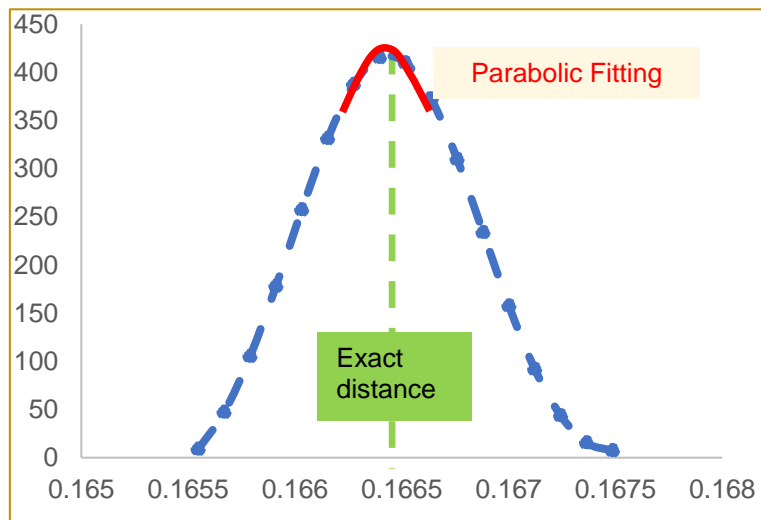
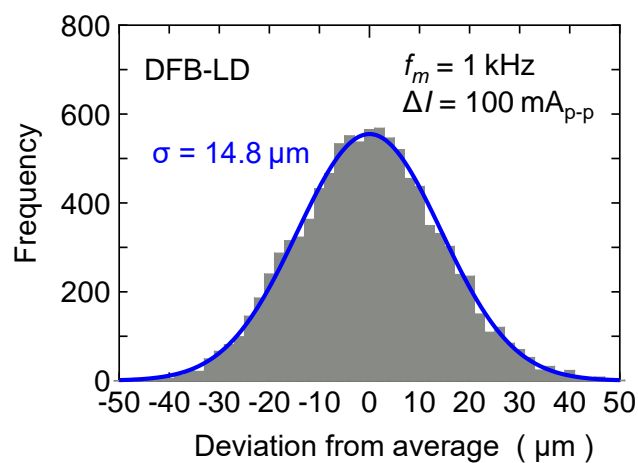
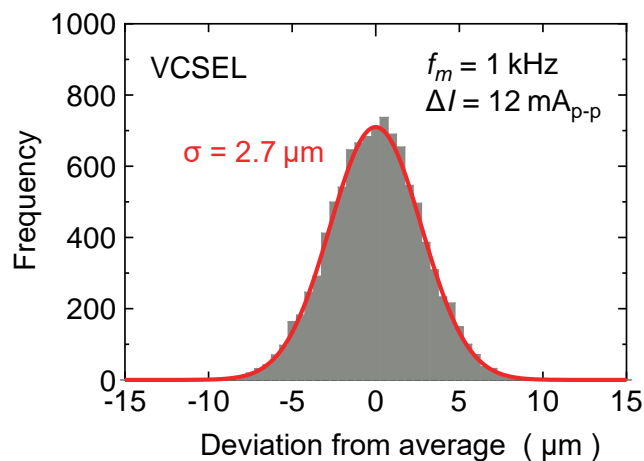


Figure 4.4 Parabolic fitting to obtain the exact distance.

To evaluate the ranging accuracy and reliability, the ranging is repeated 10,000 times for the mirror located at 17 cm. The mirror is put on the measurement table and is not fixed on the measurement table. The histogram of the ranging error is shown in Fig. 4.5(a) when the DFB laser is used and in Fig. 4.5(b) when the VCSEL is used. In the figures, the horizontal axis is the deviation from the averaged distance, and the vertical axis is the frequency. In the figures, the solid curves are the normal distribution with the standard deviation $\sigma = 14.8 \mu\text{m}$ for Fig. 4.5 (a) and $\sigma = 2.7 \mu\text{m}$ for Fig. 4.5(b). The standard deviation when using the VCSEL is smaller than that when using the DFB laser. The result means that smaller ranging error will be achieved by using the VCSEL as the frequency swept laser source.



(a) Histogram when the DFB laser as frequency swept laser source



(b) Histogram wen the VCSEL as frequency swept laser source.

Figure 4.5 Histogram of the measured distance error for 10000-times measurements at a distance of 17 cm.

Figure 4.6 shows the correlation between the measured FWHM and the standard deviation. In the figure, the closed red circles are the results when using the VCSEL with different modulation amplitudes, and the close blue square is the result when using the DFB laser with the modulation amplitude of 100 mA_{p-p}. The red solid line is a linear regression curve. The repetition of the frequency of the injection current modulation is 1 kHz for all the measurements. Figure 4.6 explains that the standard error, that is the ranging error, is proportional to the FWHM. By enhancing the spatial resolution, the highly accurate object profiling can be achieved.

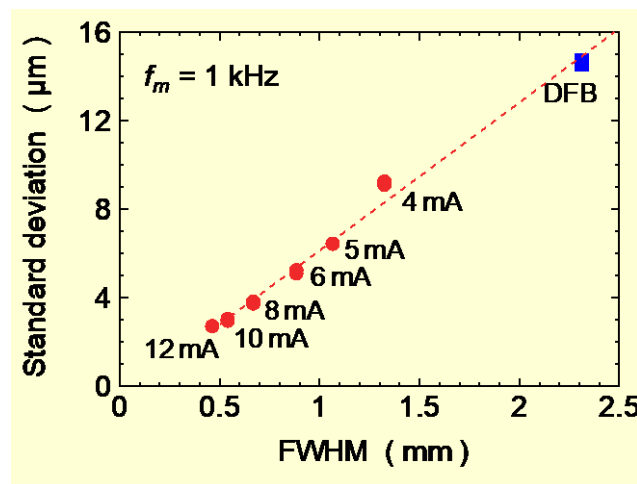


Figure 4.6 Relationship between the FWHM and the standard deviation.

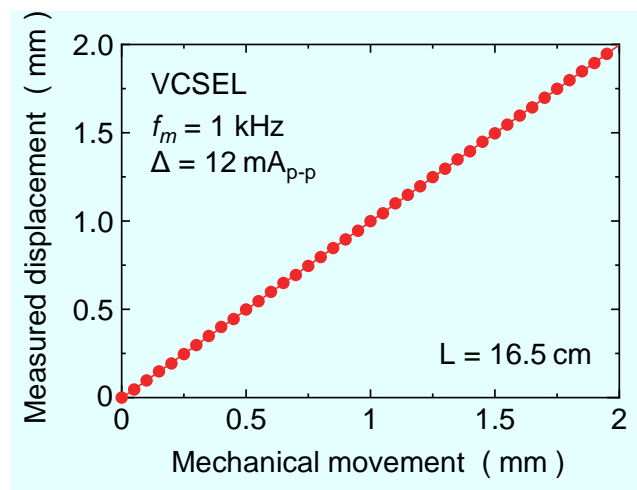


Figure 4.7 Measured displacement against the small displacement.

Next we measured the beat spectrum and the distance when the location of the mirror is slightly changed to confirm that whether small distance can be accurately measured. The location of the mirror is slightly changed with 50 μm interval around 16.5 cm. The result is

shown in Fig. 4.7. The measured distance agrees well with the mechanical movement, and then the displacement is found to be accurately measured. From Figs. 4.5 ~ 4.7, we expected that clear profiling of small object such as workpieces will be achieved by our purpose system.

4.2 Object Profiling

In section 4.1, we explained that high spatial resolution and small error ranging can be realized by using the VCSEL as the frequency swept laser source, and highly accurate object profiling and clearly object profiling is expected. In this section, the quality of profiling results of a 100 Japanese 100YEN coin when using the DFB laser and using the VCSEL is compared. By using the two-dimensional Galvano mirror, the laser light is changed from -2.5° to $+2.5^\circ$ in 0.025° increment and the corresponding profiled area is $26.5 \times 26.5 \text{ mm}^2$.

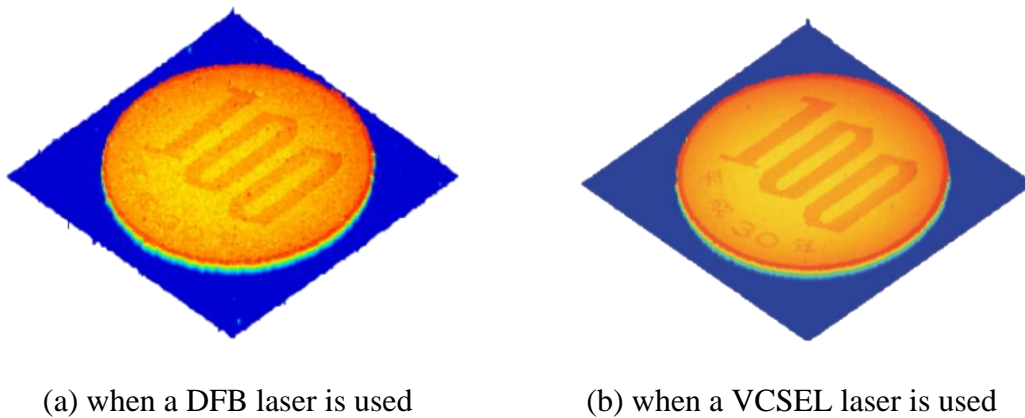


Figure 4.8 Three-dimensional profiling result of a Japanese 100YEN coin.

Figure 4.8 shows the object profiling of a Japanese 100YEN coin; (a) when the DFB laser is used and the number of acquired data is 450 points, (b) when the VCSEL is used and the number of acquired data is 2350 points. The number of FFT analysis is 4096 points by using zero padding method. The profiled data is 201×201 points, and the measurement time is about 42 sec. The object profiling in (b) is clearer than (a), and then it is concluded that the clear profile is achieved by using the VCSEL as the frequency swept laser source. Based on the histogram shown in Fig. 4.5, the VCSEL has a higher spatial resolution compared to the DFB laser and the smaller measurement error is achieved as a result. It is also found that the incuse on the surface of the coin (labels “100” and Japanese traditional era name) is successfully profiled by using the VCSEL as the frequency swept laser source.

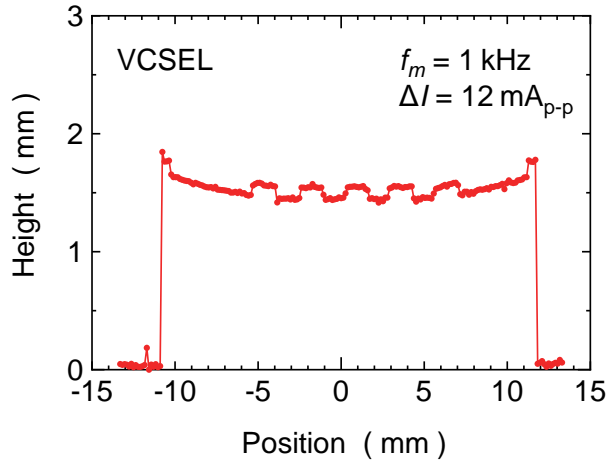
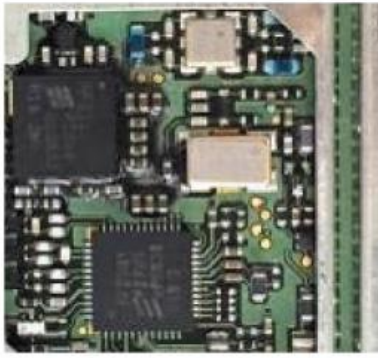


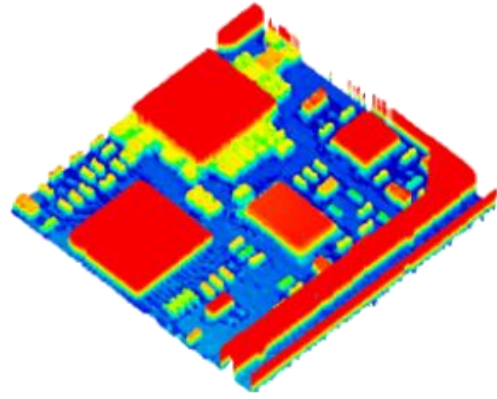
Figure 4.9 Two-dimensional profiling result around the center of a Japanese 100YEN coin.

The developed system can be used not only profiling an object but also measurement the thickness of the object. Figure 4.9 shows the two-dimensional profile around the center of the Japanese 100YEN coin. The thickness at the edge of the coin is 1.7 mm and is 1.5 mm at the center, and the surface of the coin is slightly curved. The step height of the label “100” is clearly measured to be 100 μm . We can observe five steps in the two-dimensional profiling object, which indicate the label of “100”. The standard deviation when the VCSEL is used as frequency swept laser source is 2.7 μm as shown in Fig. 4.5 (b) and is smaller than the step height of the incuse. So, the step height of incuse on the Japanese 100YEN coin is successfully measured.

We have successfully profiled the coin as shown in Fig. 4.9. Since the coin is made from the metal, the surface has strong relatively to reflect the light, and then the large-amplitude interference signal can be easily obtained. To demonstrate that the purpose system can be applied not only the object that made of metal, but also the object with low-surface reflectivity such as a glass and a plastic. A printed circuit board is chosen as an alternative object, and the profiling result is presented in Fig. 4.10. The plastic-packaged ICs and chip components are profiled, and narrow wirings between ICs and chip components are also profiled. The width of the narrow wiring is about 80 μm , and then the beam size on the target is deduced to be a few tens μm . We can then conclude that the proposed system is also applicable to inspection in the mechanical and electrical assembly process.



(a) Photograph



(b) Profiled Result

Figure 4.10 Photograph and three-dimensional profiling result of a printed circuit board.

4.3 Short Measurement Time Object Profiling

4.3.1 Without optimizing timing method

In the previous section, the FMCW optical ranging system used the VCSEL as the frequency swept laser source is very useful for object profiling, and a Japanese 100YEN coin was successfully profiled with the measurement time is 42 sec with 201 x 201 points using $f_m = 1$ kHz. To achieve shorter measurement time, the repetition frequency of the injection current modulation f_m should be increased. Here we compare two methods, i.e. without optimizing timing shows in section 4.3.1 and with optimizing timing shows in section 4.3.2.

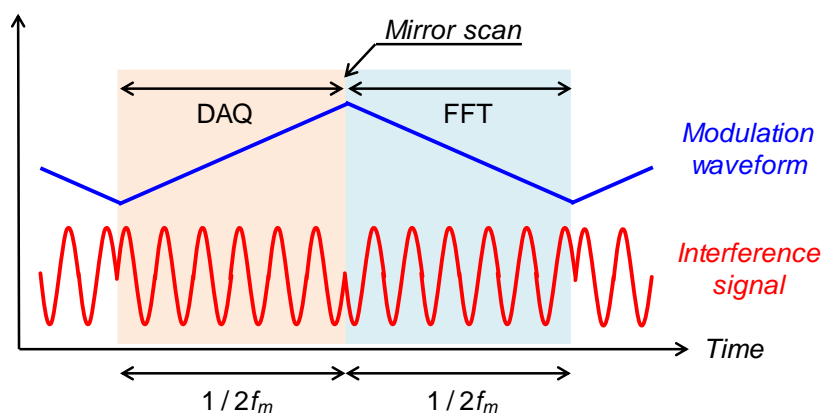


Figure 4.11 Timing without optimizing timing method.

Figure 4.11 shows the timing of the data acquisition (DAQ), the Galvano mirror scan and the FFT analysis. The optical frequency of the laser source is swept by modulating the

injection current with the asymmetric triangular signal. The interference signal in the increasing section of the modulation waveform is acquired, and the Galvano mirror is scan to the next position after the data acquisition, and then the acquired data is analysis by FFT. As a result, one distance measurement is completed within the period of $1/f_m$. In this method, the data acquisition (DAQ) time is the same with the time of the FFT analysis. When the repetition frequency of the injection current modulation $f_m = 1$ kHz, the theoretical measurement time is 40.4 sec ($201 \times 201 \times 1$ ms). The total processing time of the data transfer from AD board to the computer and the following data analysis including the FFT is less than 250 μ s, and then the repetition frequency of the injection current modulation up to $f_m \leq 2$ kHz is expected to generate the object profile without time delay.

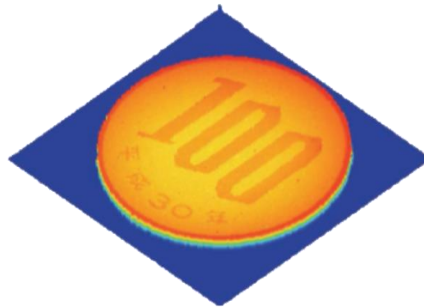


Figure 4.12 Three-dimensional profiling result of a Japanese 100YEN coin without optimizing timing for $f_m = 1$ kHz.

By using this method and using the VCSEL as the frequency swept laser source, the three-dimensional profiling of a Japanese 100YEN coin shows in the Fig 4.12. The profile is generated with $f_m = 1$ kHz, 2350 points of the number of the data acquisition the number and 4096 points of the number of the FFT analysis. The resultant profiled data is 201 x 201 points with the measurement time is 42 sec, which is almost the same with the theoretical measurement time.

The transient property of the Galvano mirror is another factor of determining the speed of the measurement. Figure 4.13 represents the small signal step response of the Galvano mirror. The angle of the mirror is 0.1 degrees if the input voltage to the Galvano mirror is 100 mV. The step response of the Galvano mirror is delayed with respect to the input signal. The time to stabilize the scan of the Galvano mirror is more than 350 μ s, and the scan of Galvano mirror is stable 400 ~ 600 μ s after the input voltage change. This means that the maximum repetition

frequency of the injection current modulation $f_{m(\max)}$ is given as $f_{m(\max)} \approx \frac{1}{2 \times 350 \mu\text{s}} = 1.4 \text{ kHz}$ for the symmetric modulation waveform.

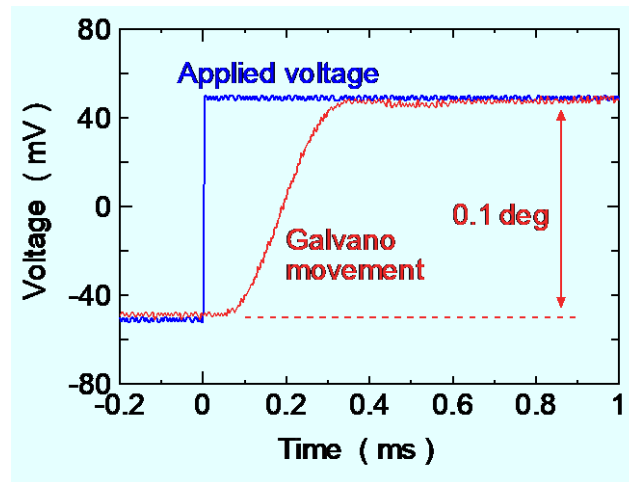


Figure 4.13 Step response of the Galvano mirror.

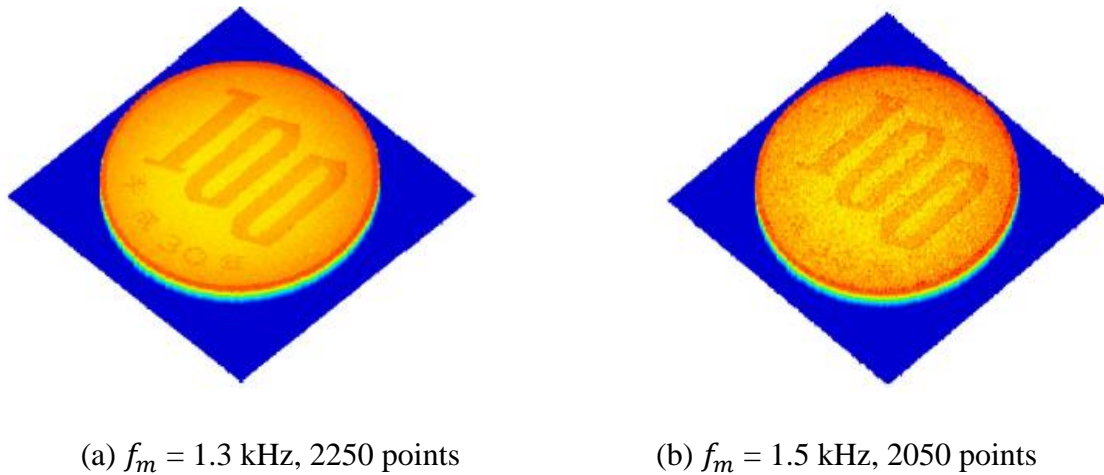


Figure 4.14 Three-dimensional profiling result of a Japanese 100YEN coin using without optimizing timing method and the VCSEL as the laser source.

Based on the value of $f_{m(\max)}$, the object profiling for a Japanese 100YEN coin is performed for the repetition frequency of the injection current modulation $f_m = 1.3 \text{ kHz}$ and $f_m = 1.5 \text{ kHz}$. Due to the limited operation speed of the k -sampling clock generator, the modulation current amplitude ΔI for $f_m = 1.5 \text{ kHz}$ is reduced to $\Delta I = 11 \text{ mA}_{\text{p-p}}$. The measured profiling result of a Japanese 100YEN coin is shown in Fig 4.14 for (a) $f_m = 1.3 \text{ kHz}$ and (b) $f_m = 1.3 \text{ kHz}$. The number of the acquired data is 2250 point and 2050 point for (a) and (b), respectively. The number of points for FFT analysis is 4096 points. The clear profile is obtained when $f_m = 1.3 \text{ kHz}$ as shown in Fig 4.14(a), and the profiling result for $f_m = 1.5 \text{ kHz}$ is noisy

as shown in the Fig 4.14(b) because of the repetition frequency of the injection current modulation $f_m > f_{m(\max)}$. The measurement time for $f_m = 1.3$ kHz is 34 sec.

4.3.2 With optimizing timing method

To improve the profiling quality for high repetition frequency of the injection current modulation f_m , the number of data acquired is decreased. The optimized timing of the data acquisition (DAQ), the Galvano mirror scan and the FFT analysis is shown in Fig. 4.15. In this method, the data acquisition (DAQ) time is not equal to the time of the FFT analysis, and the time for the FFT analysis is longer than the data acquisition time. The data acquisition is finished before the turning point of the modulation signal, and then the Galvano mirror is immediately scanned to the next position. This condition provides causes enough for stabilizing the transient response of the Galvano mirror.

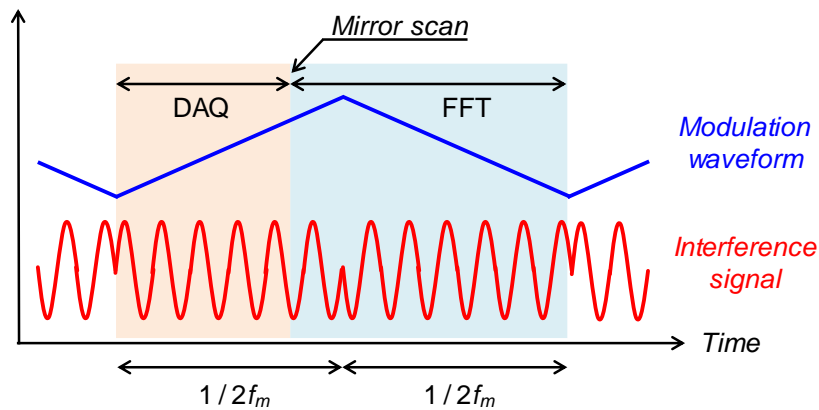
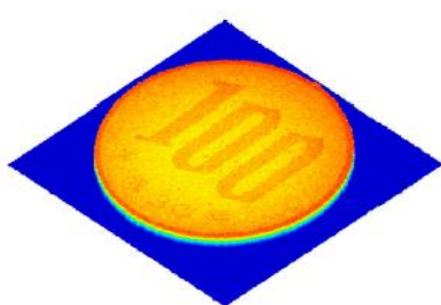


Figure 4.15 Timing with optimizing timing method.



(a) $f_m = 1.5$ kHz, 1850 points



(b) $f_m = 1.5$ kHz, 1650 points

Figure 4.16 Three-dimensional profiling result of a Japanese 100YEN coin with reduced number of acquired data for $f_m = 1.5$ kHz.

Figure 4.16 shows the result of the object profiling for $f_m = 1.5$ kHz with optimizing timing. The number of the acquired data is (a) 1850 points and (b) 1650 points, which is 200 points and 400 points fewer than the number of the acquired data for Fig. 4.14(b). Clear object profiling is achieved by reducing the number of the acquired data as shown in Fig. 4.16 because the transient behavior of the Galvano mirror becomes more stable.

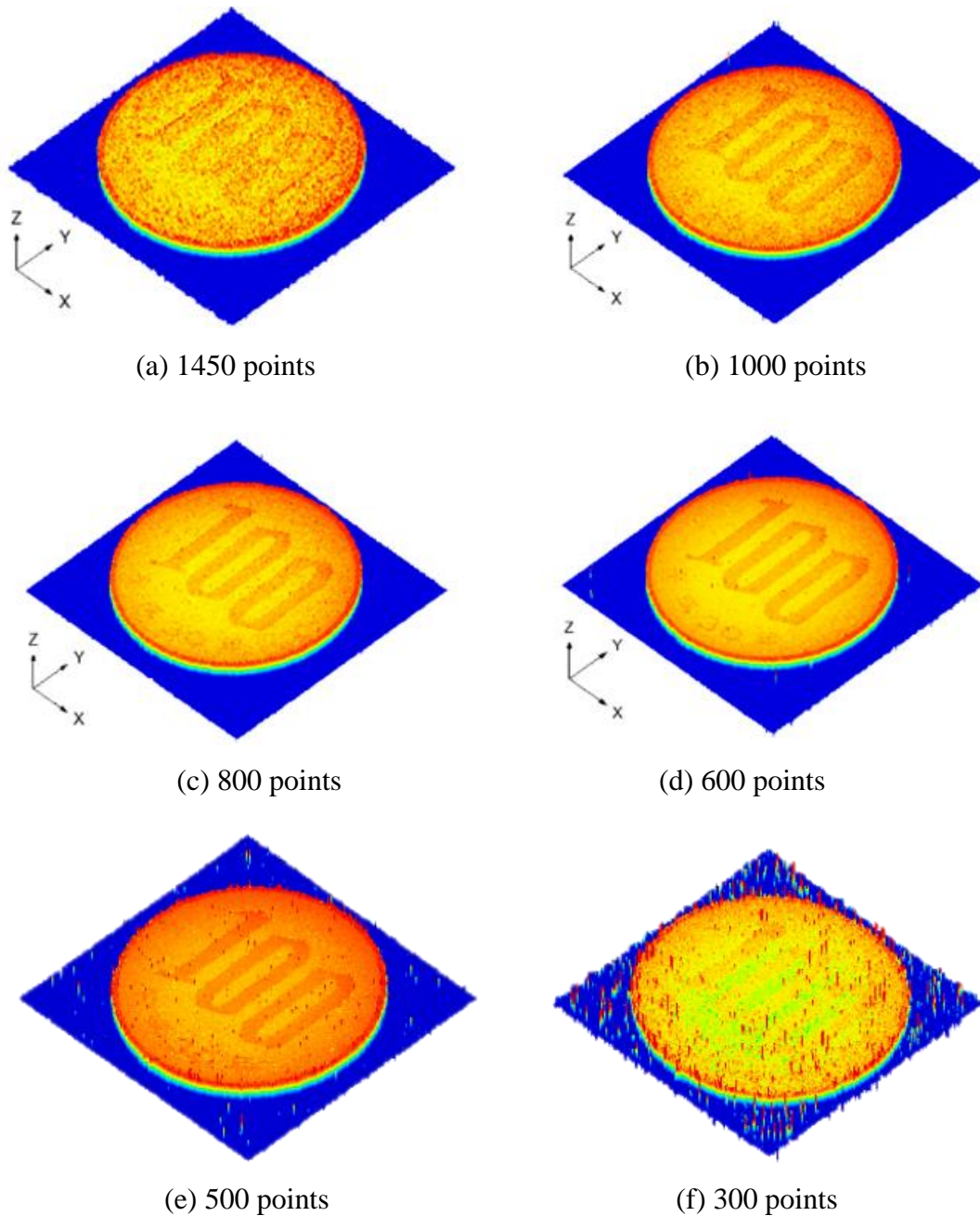


Figure 4.17 Three-dimensional profiling result of a Japanese 100YEN coin with different number of acquired data for $f_m = 1.8$ kHz.

Next we profiled a Japanese 100YEN coin to find out the required number of the acquired data for clear profiling and higher repetition frequency of the injection current modulation to speed-up the measurement time. Figure 4.17 shows the profiling result when the repetition frequency of injection current modulation $f_m = 1.8$ kHz. The number of the acquired data is (a) 1450 points, (b) 1000 points, (c) 800 points, (d) 600 points, (e) 500 points, and (f) 300 points. The number of points for the FFT analysis is 4096 points. Because the limited operation speed of the k -sampling clock generator, the modulation current amplitude is reduced to $\Delta I = 8$ mA_{p-p}. The object profiling shown in (a) and (f) are very noisy, and many spike noise are observed in (b), (c) and (e). However, decreasing the number of the acquired data is not always capable to achieve clear object profiling. On the evidence, the profiled result shown in Fig. 4.17(e) and (f) are not clear even though the number of the acquired data is more reduced. Although the quality of object profiling becomes basically clear by decreasing the number of the acquired data, there is an optimum number of the acquired data for clear profiling. The clearer 3D profile is achieved when the number of acquired data is 600 points as shown in Fig. 4.17(d), because enough time is provided for stabilizing the transient response of the Galvano mirror by decreasing the number of acquired data.

Even though the decreasing number of acquired data is sufficient to speed-up the measurement time with high quality as shown in Fig. 4.17, the optical frequency sweep range ΔF is also reduced, and then the spatial resolution and the ranging accuracy are degraded. The 600 points of acquired data corresponds to the effective optical frequency sweep range $\Delta F \approx 180$ GHz, and the FWHM of the beat spectrum and the ranging accuracy can be deduced to be 1.67 mm and about 10 μ m from eq. (6) and Fig 4.6. The ranging accuracy is still better than that when DFB laser used as the laser source, and as a result, the profiling result is clearer than the result when the DFB laser is used as the frequency sweep laser source as shown the Fig. 4.8(a). By applying the optimizing timing method, the proposed system can generate clear profiling of a Japanese 100YEN coin with the measurement time of 22.6 sec, which is about 4 times faster than our previous result reported in [9].

Increasing the repetition frequency of the injection current modulation f_m is not always a solution for clear profiling in short measurement time. The experimental result of the object profiling for the repetition frequency of the injection current modulation $f_m = 2.0$ kHz and the modulation current amplitude $\Delta I = 8$ mA is shown in Fig. 4.18. Figure 4.18(a) and (b) are the result when the number of the acquired data is 1400 points and 800 points, respectively. The quality of the object profiling is very bad, and the label “100” on the coin cannot be recognized.

The measurement time for Fig 4.18(a) is 40.718 sec. Although the quality of the object profiling becomes slightly improved by decreasing the number of the acquired data from 800 points to 700 and 500 points, the profiling results is still hard noisy as shown in Fig.4.18(c) and (d). The measurement time for 800 points of the number of the acquired data and 4096 points of the number of the FFT analysis is 20.5 sec. This measurement time is shorter than that when $f_m = 1.8$ kHz, but the profiled result is not as clear as the profiled result when $f_m = 1.8$ kHz.

It is proved that the clear object profiling of a Japanese 100YEN coin will be achieved when the repetition frequency of the injection current modulation f_m is 1.8 kHz.

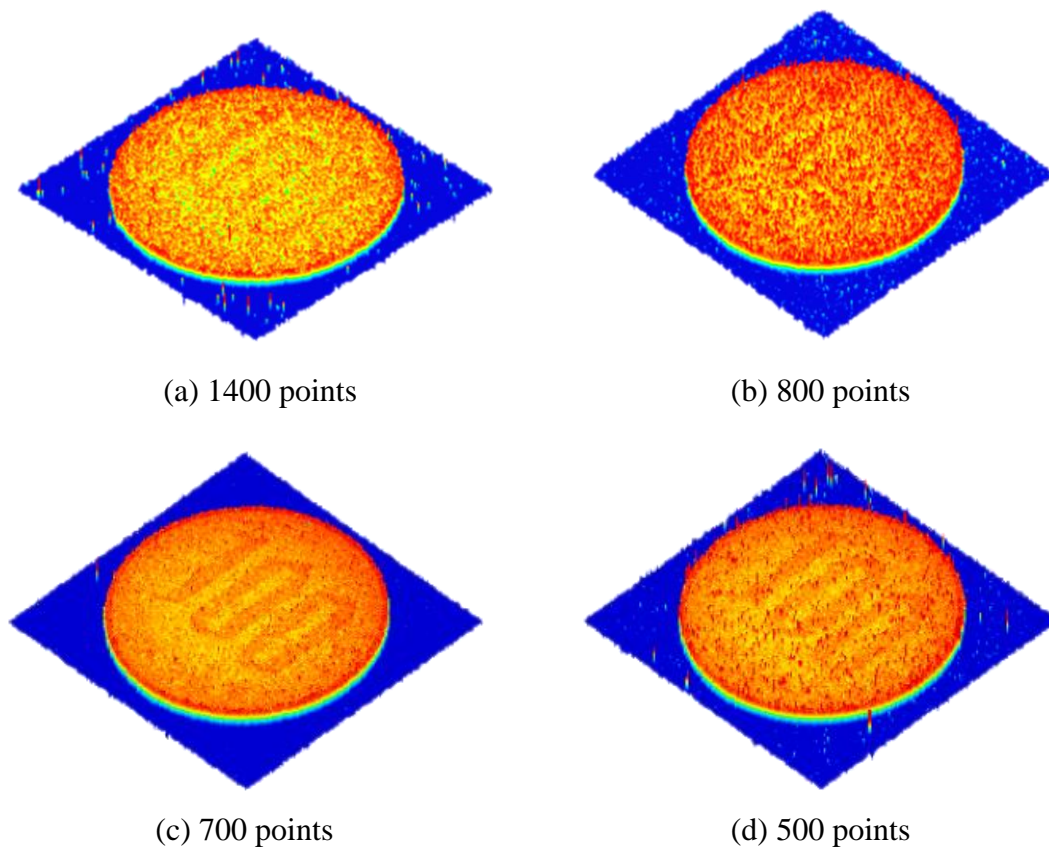


Figure 4.18 Three-dimensional profiling result of a Japanese 100YEN coin with different number of acquired data for $f_m = 2.0$ kHz.

4.4 Symmetric and Asymmetric Method

4.4.1 Symmetric Method

A symmetric triangular signal was used as the modulation signal as shown in Fig. 4.19 in the previous experiments. The increasing section in the modulation waveform was used for the data acquisition (DAQ) and the decreasing section used for the FFT analysis. In the

symmetric method, the period of $1/f_m$ is divided into two-part with the same portion. When the repetition frequency of the injection current modulation f_m is 1 kHz, 500 μ s is used for the data acquisition analysis and the following 500 μ s is for the FFT analysis.

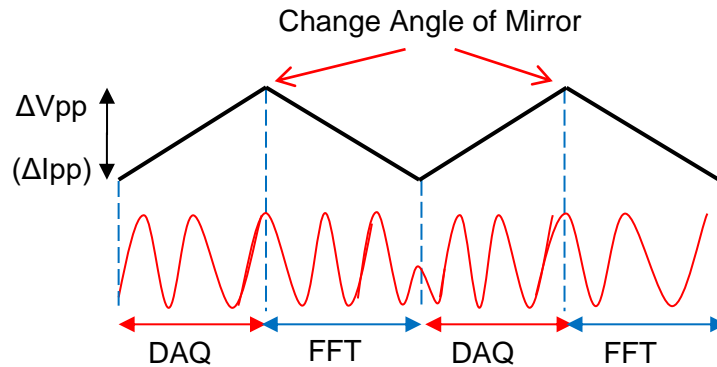
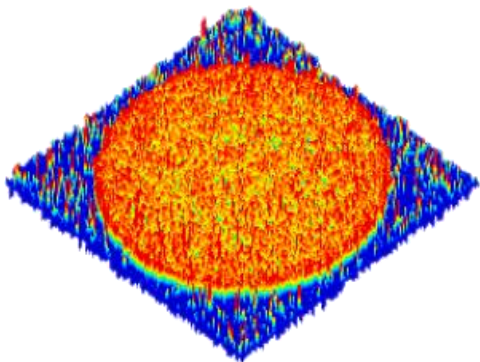
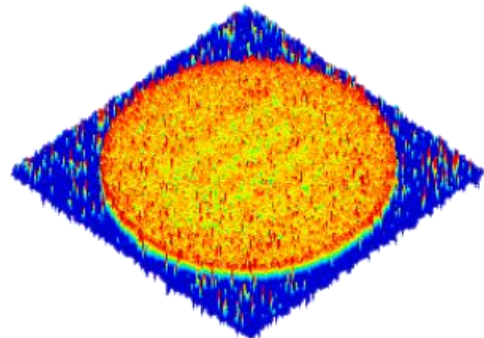


Figure 4.19 Analysis of data signal using the symmetric method

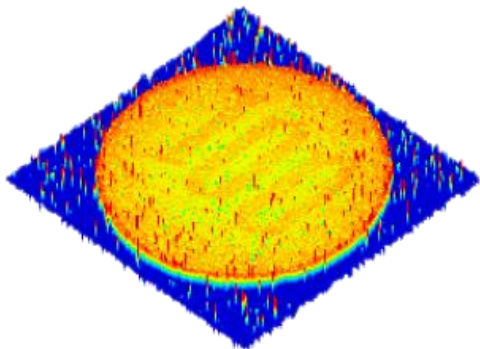
Figure 4.20 shows the object profiling result of a Japanese 100YEN coin using the symmetric method with the modulation amplitude ΔI is 8 mA. The number of the data for the FFT analysis is 4096 points. The number of the acquired data is 650 points for (a) ~ (h) and is 300 points for (i) and (j). All the profiled results are not clear as shown in Fig. 4.20. However, the profiling result for $f_m = 1.8$ kHz is slightly clear as compared to the other result.



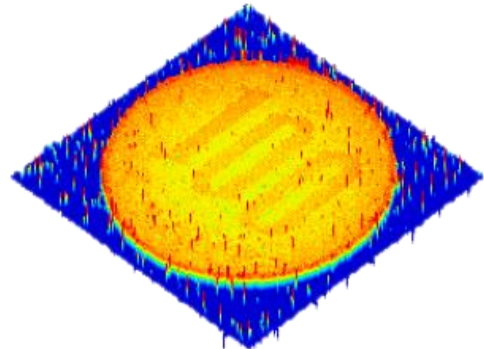
(a) $f_m = 1$ kHz, 650 points, 40.9 sec



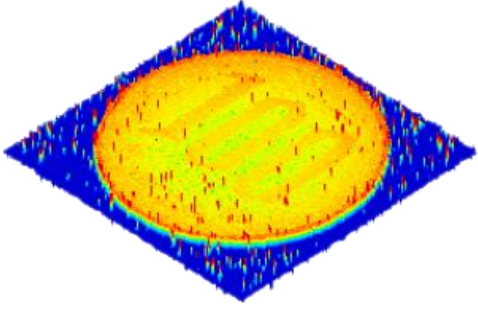
(b) $f_m = 1.1$ kHz, 650 points, 37.2 sec



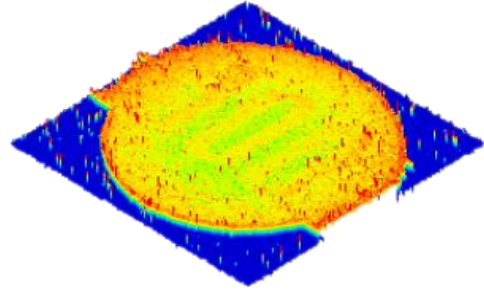
(c) $f_m = 1.2$ kHz, 650 points, 34.3 sec



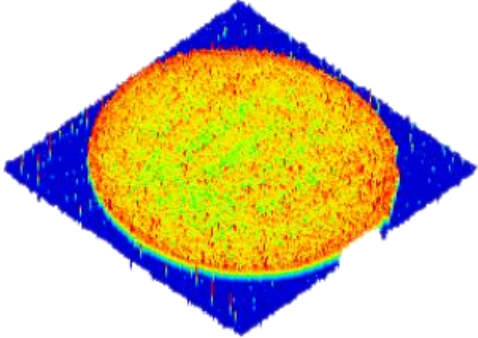
(d) $f_m = 1.3$ kHz, 650 points, 31.329 sec



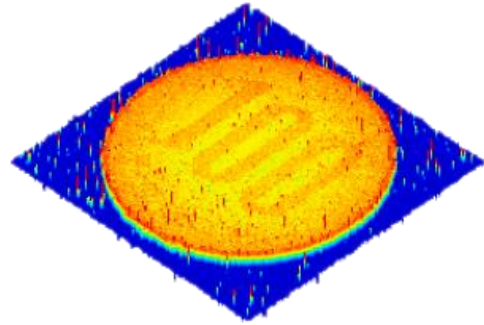
(e) $f_m = 1.4$ kHz, 650 points, 30.082 sec



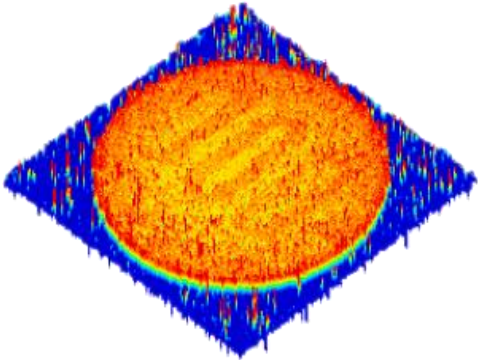
(f) $f_m = 1.6$ kHz, 650 points, 27.166 sec



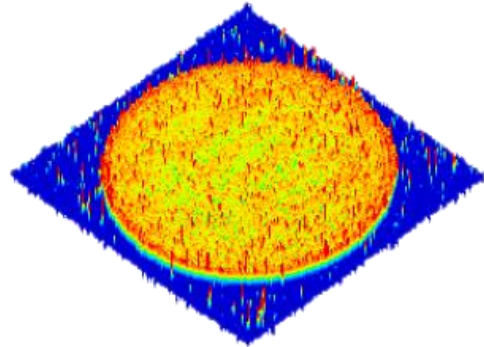
(g) $f_m = 1.7$ kHz, 650 points, 25.812 sec



(h) $f_m = 1.8$ kHz, 650 points, 23.025 sec



(i) $f_m = 1.7$ kHz, 300 points, 21.59 sec



(j) $f_m = 1.8$ kHz, 300 points, 20.704 sec

Figure 4.20 Three-dimensional profiling result of a Japanese 100YEN coin using the symmetric method with a different repetition frequency of the injection current modulation.

The profiled data in this experiment is 201×201 points. The theoretical measurement time is given as:

$$\text{Measurement time} = \text{Total data number} \times (T_r + T_f) \quad (14)$$

where T_r and T_f are increasing and decreasing periods, respectively.

The theoretical and the experimental measurement times for profiling a Japanese 100YEN coin by using the symmetric method for $f_m = 1$ kHz, 1.1 kHz, 1.2 kHz, 1.3 kHz, 1.4 kHz, 1.6 kHz, 1.8 kHz and 2.0 kHz are shown in Fig. 4.21. The measurement time is inversely proportional to the repetition frequency of the injection current modulation. Considering the short measurement time and clear profiling result in the symmetric method, the clear and the fastest condition is $f_m = 1.8$ kHz, 650 points of the number of the acquired data, and 4096 points of the number for the FFT analysis, and the resultant measure time is 23.1 sec.

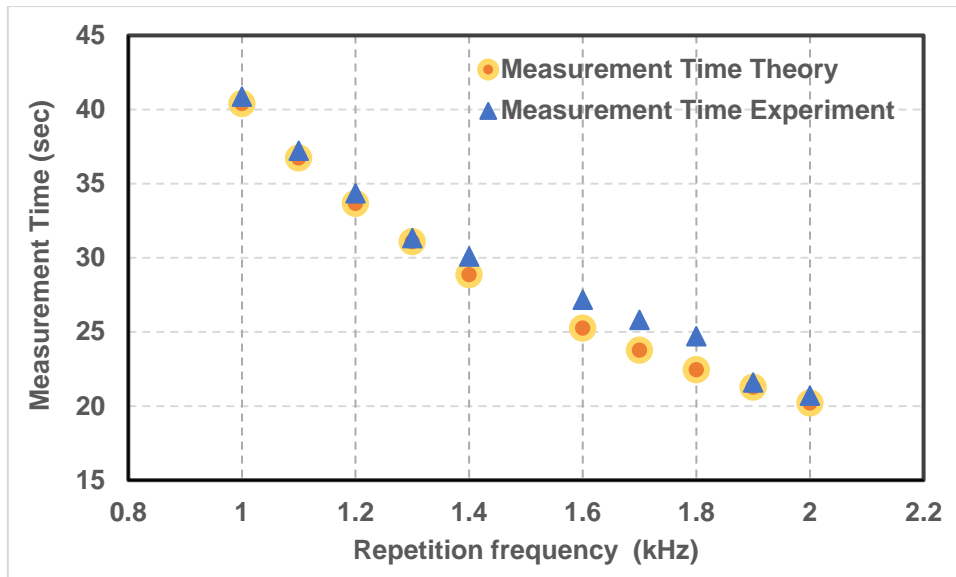


Figure 4.21 Relationship between the repetition frequency of the injection current modulation and the measurement time.

4.4.2 Asymmetric Method

Figure 4.22 shows the timing when using an asymmetric modulation waveform. The increasing section of the modulation waveform is used for data acquisition (DAQ) and the decreasing section is used for the FFT analysis, where T_r and T_f are the periods of the increasing section and the decreasing section is falling, respectively. In the asymmetric method, the increasing period and the decreasing period are not the same.

Figure 4.23 shows the object profiling result for $f_m = 1.0$ kHz, $T_r = 620 \mu\text{s}$, and $T_f = 380 \mu\text{s}$. The profiling result is clear, however the measurement time is as long as 67.6 sec. In this experimental condition, enough time is provided for stabilizing the transient response of the Galvano mirror, which determines the measurement speed of the object profiling.

Determination of the increasing and the decreasing periods in the injection current modulation contributes to stability of the transient response of the Galvano mirror. In the previous section, we demonstrated that the Galvano mirror scanner requires more than 350 μs for stabilizing. Based on the theoretical measurement time shown in Fig 4.21 and the profiling result using the symmetric method, the fine object profiling is achieved at $f_m = 1.8 \text{ kHz}$ with the measurement time for about twenty sec. The asymmetric method can be useful for fast and clear object profiling, and then the profiling of a Japanese 100YEN coin is carried out for the repetition frequency of the injection current modulation of 1.8 kHz ~ 2.0 kHz. The increasing section is used for the data acquisition and the stabilizing the transient property of the Galvano scanner, and the period of the decreasing section is kept longer than 350 μs to stabilize the transient property of the Galvano scanner.

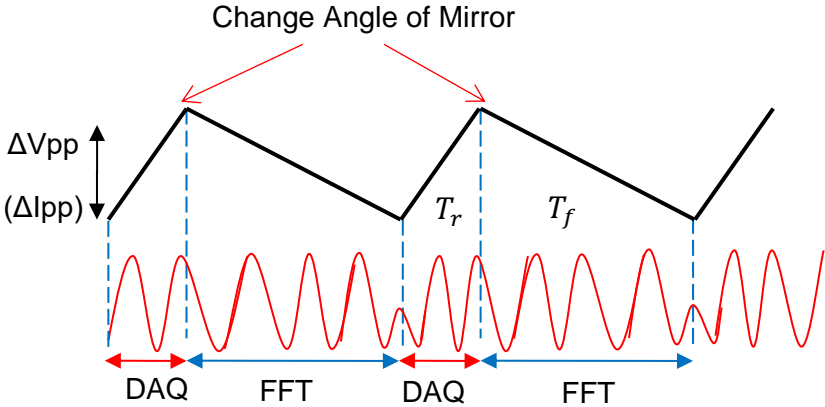
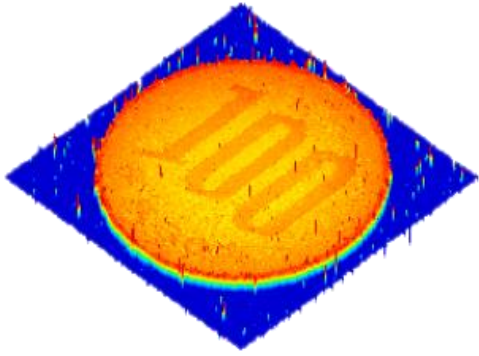


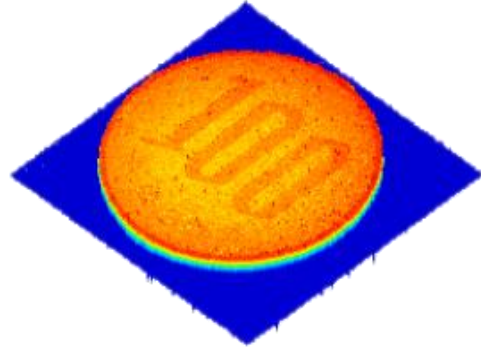
Figure 4.22 Timing of the data acquisition and the FFT analysis for the asymmetric method.



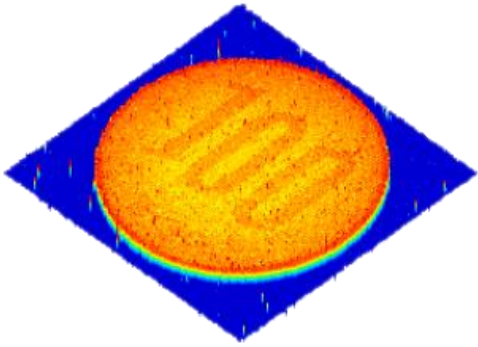
Figure 4.23 Three-dimensional profiling result of a Japanese 100YEN coin using the asymmetric method with $f_m = 1.0 \text{ kHz}$, $T_r = 620 \mu\text{s}$, $T_f = 380 \mu\text{s}$ and the number of acquired data is 1650 points.



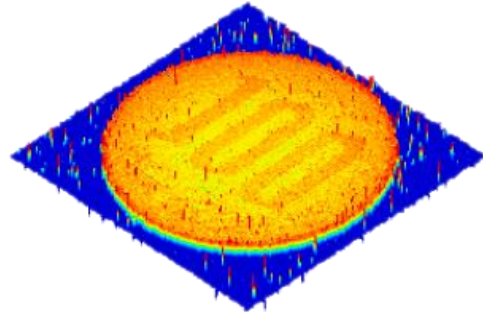
(a) $f_m = 1.8$ kHz; $T_r = 155$ μ s;
 $T_f = 400$ μ s; 380 points; 22.6 sec



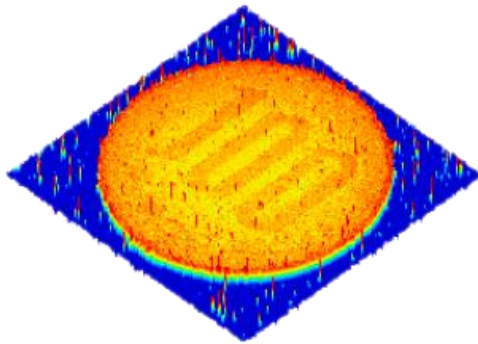
(b) $f_m = 1.8$ kHz; $T_r = 165$ μ s;
 $T_f = 390$ μ s; 650 points; 22.6 sec



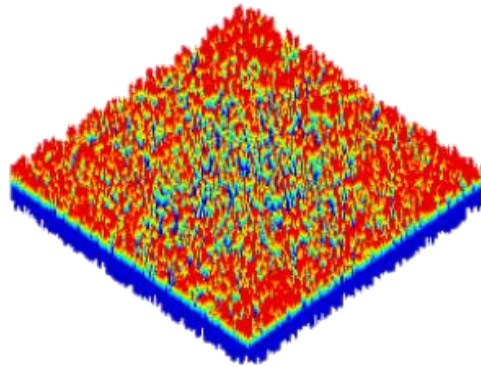
(c) $f_m = 1.82$ kHz; $T_r = 170$ μ s;
 $T_f = 380$ μ s; 650 points; 22.6 sec



(d) $f_m = 1.96$ kHz; $T_r = 130$ μ s;
 $T_f = 380$ μ s; 380 points; 20.9 sec



(e) $f_m = 2.0$ kHz; $T_r = 120$ μ s;
 $T_f = 380$ μ s; 420 points; 20.4 sec



(f) $f_m = 2.0$ kHz; $T_r = 100$ μ s;
 $T_f = 400$ μ s; 500 points; 20.5 sec

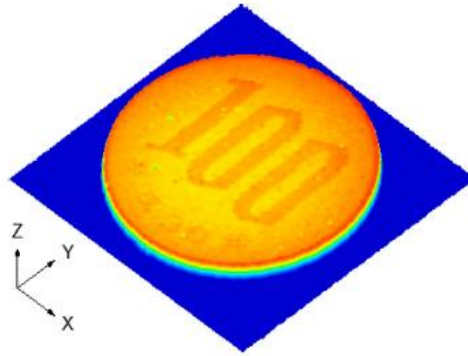
Figure 4.24 Three-dimensional profiling result of a Japanese 100YEN coin using the asymmetric method with different f_m and periods in the increasing and the decreasing sections.

Figure 4.24 shows the profiling result of a Japanese 100YEN coin using the asymmetric method with different repetition frequency of the injection current modulation f_m , the increasing period T_r , and the decreasing period T_f . The profiled results shown in (a), (b) and (c) has less noise as compared to the profiled results shown in (d), (e) and (f). It means that the FMCW optical ranging system with VCSEL is capable to generate the clear profile when the repetition frequency of the injection current modulation is about 1.8 kHz, and the measurement time is 22.6 sec. Although Figs. 4.24(d), (e) and (f) have shorter measurement time of about 20 sec, the profiling result is not clear, when f_m is more than 1.9 kHz. Figure 4.24(a) is the result when the increasing and the decreasing periods are 155 μ s and 400 μ s, respectively. The profiled result is clearer compared to Figs. 4.24(b) and (c).

4.5 Filtering

Although decreasing the number of the acquired data is effective to achieve clear profile, some spike noise still is observed in the Fig. 4.17(d). The spike noise can be eliminated by filtering. In this experiment, three types of filtering are examined: (a) a 3 x 3 moving average filter, (b) a 3 x 3 median filter and (c) a 3-points median filter for x -direction. The filtering results of the three-dimensional profile of a Japanese 100YEN coin are shown in Fig. 4.25. Figure 4.25(a) is the filtered profiling result using a 3 x 3 moving average filter to Fig. 4.17(d). Although the spike noise is eliminated, the profiling result is blurred. The results of the median filtering are shown in Fig. 4.25(b) and (c). The spike noise is eliminated and the profiling results are clearer than Fig. 4.25(a). It is also found that the profiling result shown in Fig. 4.25(b) is slightly blurred and the clear object profiling is achieved by applying a 3-points median filtering for x -direction as shown in Fig. 4.25(c).

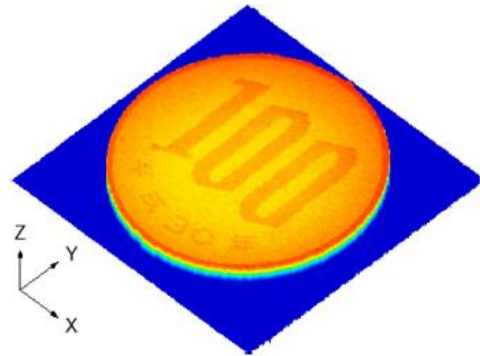
Applying a 3-points median filter for y -direction gives similar profiling result with Fig. 4.25(c). The optimal type of a filter depends on surface profile of an object to be profiled. A moving average filter is a kind of a low pass filter, and then step-like surface profile is smoothed and blurred. Therefore, a moving average filter is effective for profiling an object which has smooth surface without step-like surface profile.



(a) 3 x 3 moving average filter



(b) 3 x 3 median filter

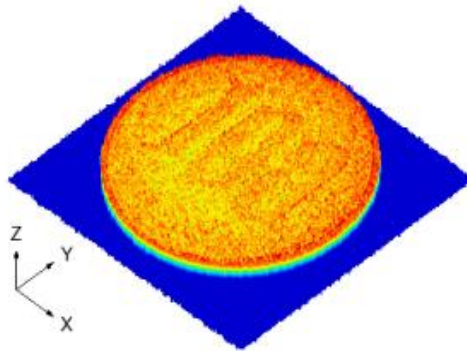


(c) 3-points median filter for x -direction

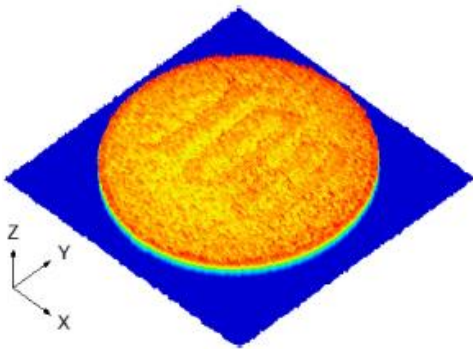
Figure 4.25 Three-dimensional profiling result of a Japanese 100YEN coin after different types of filtering with $f_m = 1.8$ kHz and the number of acquired data is 600 points.

A median filter is widely used to eliminate noise without blurring because no averaging is used. Therefore, a median filter is effective for profiling an object which has step-like surface profile such as coin and mechanical workpieces. We tried to apply a 3 x 3 median filter and a 3-points median filter for x -direction, and which median filter is effective to eliminate the noise of profiling results depends on the shape and the size of step-like profile an object to be profiled.

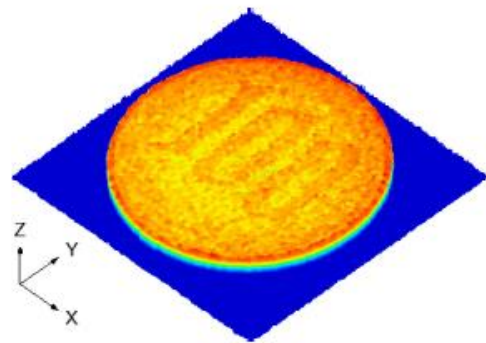
Finally, to confirm effectiveness of median filtering to noisy profiling result as shown in Fig. 4.17(a), we applied a 3-points median filter for x -direction and a 3 x 3 median profile. The original profiling result is shown in Fig. 4.26(a), and the filtered profiling results are shown in Fig. 4.26 (b) and (c), respectively. However, the filtered profiling result is still degraded as compared to the filtered profiling results shown in Fig. 4.25(b) and (c). This means that a median filtering is effective to eliminate spike noise and is insufficient for noisy profiling result.



(a) 1450 points, without filtering



(b) 1450 points, with 3-points median filter for x -direction



(c) 1450 points, 3 x 3 median filter

Figure 4.26 Three dimensional profiling result of a Japanese 100 YEN coin (a) without filtering (b) by 3-points median filter for x -direction and (c) by 3 x 3 median filter.

Chapter 5

Summary

Three-dimensional object profiling by the FMCW optical ranging system using a VCSEL as a laser source and a two-dimensional Galvano mirror are proposed and demonstrated. The laser light is scanned over a target to be profiled and the reflected light interferes with the reference light. The beat spectrum of the interference signal is analyzed by the FFT. By using a VCSEL as the frequency-swept laser source, high spatial resolution and highly accurate ranging can be achieved because of large optical frequency sweep range. The experimental spatial resolution estimated by the FWHM of the beat spectrum is 460 μm and the standard deviation of the measurement error is 2.7 μm . We also succeed to three-dimensional profile of a Japanese 100YEN coin and a printed circuit board by using the proposed sensing system, and also succeed to measure the thickness of a Japanese 100YEN coin, which is 1.7 mm at the edge of the coin and 1.5 mm at the center of the coin. The short measurement time is achieved by increasing the repetition frequency of the injection current modulation and optimizing timing of the data acquisition, the Galvano mirror scan and the FFT analysis by taking account of the transient response of the Galvano mirror, and the fastest measurement time is 22.6 sec for 201 x 201 profiled points and the repetition frequency of the injection current modulation $f_m = 1.8$ kHz. The short measurement time is also achieved by using the asymmetric method, and the fastest measurement time is also 22.6 sec by using an asymmetric triangular modulation waveform with the period of the increasing section $T_r = 155$ μs , the period of the decreasing section $T_f = 400$ μs , and the repetition frequency of $f_m = 1.8$ kHz.

The quality of the profiled result is efficiently improved by using a 3 x 3 median filter and a 3-points median filter for x -direction.

The developed system is very useful for industrial application such as diagnosing the shape of components in automotive and electronic industries, and profiling of mechanical workpieces and inspection in mechanical and electrical assembly process. The developed system is a cost effective system because a VCSEL is used as the laser source and the optical frequency is swept by injection current modulation with low repetition frequency.

References

- [1] R. K. Ula, N. Yusuke, and K. Iiyama, "High speed measurement for object profiling using FMCW optical sensing system," *J. Phys. Conf. Ser.*, vol. 1191, no. 1, 2019.
- [2] H. A. and B. W. R K Ula, D Hanto, T B Waluyo, "Design of micro bending deformer for optical fiber weight sensor," *IOP Sci.*, vol. IOP Conf., no. 2017, 2017.
- [3] Yong Bai and Qiang Bai, "Fiber Optic Monitoring System," in *Subsea Pipeline Integrity and Risk Management*. Elsevier, pp. 145–165, 2014.
- [4] Francis T.S. Yu and Shizhuo Yin, "Fiber Optic Sensors", Marcel Dekker, New York-Basel, 2002.
- [5] U. Glombitza, and E. Brinkmeyer, "Coherent frequency-domain reflectometry for characterization of single-mode integrated-optical waveguides," *J. Lightwave Technol.*, vol. 11, no. 8, pp. 1377–1384, 1993.
- [6] R. K. Ula, Y. Noguchi, and K. Iiyama, "Three-Dimensional Object Profiling Using Highly Accurate FMCW Optical Ranging System," *J. Lightwave Technol.*, vol. 37, no. 15, pp. 3826–3833, 2019.
- [7] B. J. Soller, D. K. Gifford, M. S. Wolfe, and M. E. Froggatt, "High resolution optical frequency domain reflectometry for characterization of components and assemblies," *Opt. Express*, vol. 13, no. 2, p. 666, 2005.
- [8] S. Moon and E.S. Choi, "VCSEL-based swept source for low-cost optical coherence tomography," *Biomed. Opt. Express*, vol. 8, no. 2, pp. 1110–1121, 2017
- [9] K. Iiyama, T. Washizuka, and K. Yamaguchi, "Three-dimensional object profiling by FMCW optical ranging system using a VCSEL," in *2017 Conference on Lasers and Electro-Optics Pacific Rim, CLEO-PR 2017*, Singapore, pp. 1-3, August 2017.
- [10] K. Iiyama, T. Washizuka, and Y. Kimura, "Three-dimensional object profiling using FMCW optical sensing system," in *International Symposium on imaging, sensing, and optical memory 2016*, Kyoto, Japan, pp. 148–149, November 2016.
- [11] K. Iiyama, S. I. Matsui, T. Kobayashi, and T. Maruyama, "High-resolution FMCW reflectometry using a single-mode vertical-cavity surface-emitting laser," *IEEE Photon.*

- Technol. Lett.*, vol. 23, no. 11. pp. 703–705, 2011.
- [12] K. Iiyama, L. Wang, and K. Hayashi, “Linearizing Optical Frequency-Sweep of a Laser Diode for FMCW Reflectometry,” *J. Lightwave Technol.*, vol. 14, no. No.2, pp. 173–178, 1996.
- [13] T. Hariyama, P.A.M. Sandborn, M. Watanabe, and M.C. Wu, “High-accuracy range-sensing system based on FMCW using low-cost VCSEL,” *Opt. Express*, vol. 26, no. 7, pp. 9285–9297, 2018.
- [15] K. Yuksel, M. Wuilpart, V. Moeyaert, and P. Mégret, “Optical frequency domain reflectometry: A review,” *Ict. 2009 11th Int. Conf. Transparent Opt. Networks*, no. April 2014, 2009.
- [16] K. Yuksel, M. Wuilpart, V. Moeyaert, and P. Mégret, “Optical frequency domain reflectometry: A review,” in *2009 11th International Conference on Transparent Optical Networks (ICTON 2009)*, Tu.C2.5, June 2009.
- [17] N.A.B. Lazam, K. Iiyama, T. Maruyama, Y. Kimura, and N.V. Tu, “Linearization of nonlinear beat frequency in FMCW interferometry through waveform modifying technique”, *ARPJ Journal of Engineering and Applied Sciences*, vol. 10, no. 8, pp. 3817–3822, 2015.
- [18] R. Passy, N. Gisin, J.P. von der Weid, H.H. Gilgen, “Experimental and Theoretical Investigations of Coherent OFDR with Semiconductor Laser Sources,” *J. Lightwave Technol.*, vol. 12, no. 9, pp. 1622–1630, 1994.
- [20] M. Tof, Q. T. Chipset, and T. C. E. Kit, “Time-of-flight basics,” pp. 1–16, 2017.
- [21] B. J. Soller, D. K. Gifford, M. S. Wolfe, and M. E. Froggatt, “High resolution optical frequency domain reflectometry for characterization of components and assemblies,” *Opt. Express*, vol. 13, no. 2, p. 666, 2005.
- [22] K. Yuksel, M. Wuilpart, V. Moeyaert, and P. Megret, “Optical frequency domain reflectometry: A review,” *2009 11th Int. Conf. Transparent Opt. Networks*, pp. 1–5, 2009.
- [23] K. Iiyama, T. Maeda, and S. Takamiya, “Phase-decorrelated FMCW reflectometry for long optical fiber characterization by using a laser diode with modulated external cavity,” *IEICE Trans. on Electron.*, vol. E83-C, no. 3, pp. 428–434, 2000.

- [24] B. Soller, D. Gifford, M. Wolfe, and M. Froggatt, "High resolution optical frequency domain reflectometry for characterization of components and assemblies.," *Opt. Express*, vol. 13, no. 2, pp. 666–674, 2005.
- [25] A. Larsson, "Advances in VCSELs for communication and sensing," *IEEE J. Sel. Top. Quantum Electron.*, vol. 17, no. 6, pp. 1552–1567, 2011.
- [26] F. Koyama, "Advances of VCSEL photonics," *Conf. Progr. - MOC'11 17th Microoptics Conf.*, vol. 24, no. 12, pp. 4502–4513, 2011.
- [27] E. P. Haglund, P. Westbergh, J. S. Gustavsson, and A. Larsson, "Impact of damping on high-speed large signal VCSEL dynamics," *J. Lightwave Technol.*, vol. 33, no. 4, pp. 795–801, 2015.
- [28] E. Simpanen *et al.*, "1060 nm Single-Mode VCSEL and Single-Mode Fiber Links for Long-Reach Optical Interconnects," *J. Lightwave Technol.*, vol. 37, no. 13, pp. 2963–2969, 2019.
- [29] G. D. Cole, E. Behymer, T. C. Bond, and L. L. Goddard, "Short-wavelength MEMS-tunable VCSELs," *Opt. Express*, vol. 16, no. 20, pp. 16093–16103, 2008.
- [30] A. V. Naumenko, N. A. Loiko, M. Sondermann, and T. Ackemann, "Description and analysis of low-frequency fluctuations in vertical-cavity surface-emitting lasers with isotropic optical feedback by a distant reflector," *Phys. Rev. A - At. Mol. Opt. Phys.*, vol. 68, no. 3, p. 16, 2003.
- [31] D. Bimberg, "Thermal analysis of high-bandwidth and energy-efficient 980 nm VCSELs with optimized quantum well gain peak-to-cavity resonance wavelength offset," *Appl. Phys. Lett.*, vol. 111, no. 24, 2017.
- [32] C. Semiconductor and I. Forum, "Using VCSELs in 3D Sensing Applications 3D Depth Camera Becomes Pervasive," 2019.
- [33] T. Yoshikawa *et al.*, "Polarization-Controlled Single-Mode VCSEL," vol. 34, no. 6, pp. 1009–1015, 1998.
- [34] K. J. Ebeling and R. Michalzik, "VCSEL technology for imaging and sensor systems applications," *22nd Microoptics Conf. MOC 2017*, vol. 2017-Novem, pp. 20–21, 2017.
- [35] Y. Hong, J. Paul, P. S. Spencer, and K. A. Shore, "Influence of low-frequency

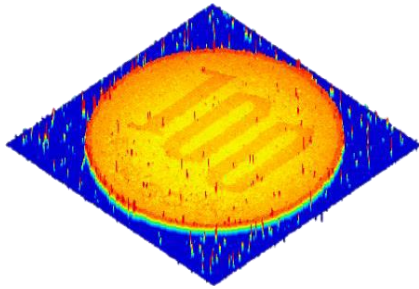
- modulation on polarization switching of VCSELs subject to optical feedback,” *IEEE J. Quantum Electron.*, vol. 44, no. 1, pp. 30–35, 2008.
- [36] K. Iiyama, T. Washizuka, and Y. Kimura, “Three-dimensional object profiling using FMCW optical sensing system,” *Int. Symp. imaging, sensing, Opt. Mem. We-K-02*, Japan, October 2016
- [37] Farhan Rana, “Distributed Feedback (DFB) Structures and Semiconductor DFB Lasers Chapter 13.”, Cornell University,
- [38] D. Feedback and S. Laser, *Principles of Distributed Feedback Semiconductor Laser Diodes* : 2003.
- [39] H. Yamazaki, M. Yamaguchi, M. Kitamura, and I. Mito, “Analysis on FM Efficiency of InGaAs / InGaAsP SCH-MQW LD ’ s Taking Injection Carrier Transport Into Account,” vol. 4, no. 4, pp. 396–398, 1993.
- [40] D. F. Lasers, *NASA Contractor Report 4154 NI \ S *, no. June 1988. 2020.
- [41] P. Hariharan, “Interferometers,” *Springer Ser. Opt. Sci.*, vol. 184, pp. 183–217, 2014.
- [42] T. Michelson, “Interferometers 2 . Michelson interferometer : theory,” pp. 1–18.
- [43] P. Giacomo, “The Michelson interferometer,” *Mikrochim. Acta*, vol. 93, no. 1–6, pp. 19–31, 1987.
- [44] R. Mehra, “Mach Zehnder Interferometer and its Applications,” pp. 31–36, 2014.
- [45] Agilent, “The Fundamentals of Signal Analysis,” *Agil. Appl. Note*, no. July, pp. 1–20, 2000.
- [46] E. O. Brigham and R. E. Morrow, “The fast Fourier transform,” *IEEE Spectr.*, vol. 4, no. 12, pp. 63–70, 1967.
- [47] Michigan State University, “Module 3 : Signals and Spectra,” *Electromagn. Compat. Course Notes*.
- [48] W. Eickhoff, “Optical frequency domain reflectometry in single-mode fiber,” vol. 693, no. August, pp. 693–695, 1981.
- [49] K. Iiyama, M. Yasuda, and S. Takamiya, “Extended-range high-resolution FMCW reflectometry by means of electronically frequency-multiplied sampling signal

- generated from auxiliary interferometer,” *IEICE Trans. Electron.*, vol. E89-C, no. 6, pp. 823–828, 2006.
- [50] D. Uttam and B. Cushlaw, “Precision time domain reflectometry in optical fiber system using a frequency modulated continuous wave ranging technique,” *J. Lightwave Technol.*, vol. LT-3, no.5, pp. 971-976, October 1985.
- [51] G. Economou, R.C. Youngquist, and D.E.N. Davies, “Limitation and noise in interferometric systems using frequency ramped single-mode diode laser,” *J. Lightwave Technol.*, vol. LT-4, no.11, pp.1601 – 1608, November 1986.
- [52] H. Barfus and Brinkmeyer, “Modified optical frequency domain reflectometry with high spatial resolution for components of integrated optic systems,” *J. Lightwave Technol.*, vol. 7, no.1, pp. 3-10, January 1989.
- [53] W.V. Sorin, D.K. Donald, S.A. Newton, and M. Narazaty, “Coherent FMCW reflectometry using a temperature tuned Nd: YAG ring laser,” *IEEE Photon. Technol. Lett.*, vol. 2, no. 12, pp. 902-904, December 1990.
- [54] L.T. Wang, K. Iiyama, F. Tsukada, N. Yoshida, and K. Hayashi, “Loss measurement in optical waveguide devices by coherent frequency modulated continuous-wave reflectometry,” *Opt. Lett.*, vol.18, no.13, pp.1095-1097, July 1993.
- [55] U. Glombitza and Brinkmayer, “Coherent frequency-domain reflectometry for characterization of single-mode integrated-optical wave-guides,” *J. Lightwave Technol.*, vol. 11, no. 8, pp. 1377 – 1384, August 1993.
- [56] R. Passy, N. Gisin, J.P. Von der Weid, and H.H. Gilgen, “Experimental and theoretical investigation of coherent OFDR with semiconductor laser source,” *J. Lightwave Technol.*, vol. 2, pp. 1622-1630, Sept. 1994.
- [57] Y. Hong, J. Paul, Paul S. Spencer, and K. Alan Shore, “Influence of low frequency modulation on polarization switching of VCSELs subject to optical feedback,” *J. of Quantum Electronic*, vol.44, no.1, pp. 30 – 35, Jan. 20
- [58] K. Iiyama, L.T. Wang, and Kayashi, “Linearizing optical frequency sweep of laser diode for FMCW reflectometry,” *J. Lightwave Technol.*, vol.14, no.2, pp. 173 -178, Feb.1996
- [59] X. Zhou, K. Iiyama, and H. Kayashi, “Extended-range FMCW reflectometry using an

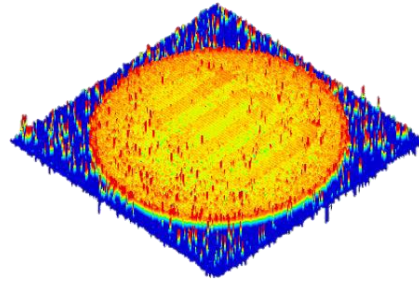
- optical loop with a frequency shifter,” *IEEE Photon. Technol. Lett.*, vol.8, no.2, pp. 248–250, Feb. 1996
- [60] J.P. von Deir Weid, R. Passy, G. Mussi, and N. Gissin, “ On the characterization of optical fiber network components with optical frequency domain reflectometry,” *J. Lightwave Technol.*, vol. 15 no. 7, pp. 1131 – 1141, July 1997.
- [61] K. Iiyama, M. Yasuda, and S. Takamiya, “Extended-range high resolution FMCW reflectometry by means of electronically frequency-multiplied sampling signal generated from auxiliary interferometer,” *IECIE Trans. Electron.*, vol. E89-C, no.6, pp. 823 – 829, June 2006.
- [62] Z. Wang, B. Potsaid, L. Chen, C. Doerr, H. C. Lee, T. Nielson, V. Jayaraman, A. E. Cable, E. Swanson, and J.G. Fujimoto, “Cubic meter volume optical coherent tomography,” *Optica*, vol. 3, issue 12, pp. 1496 – 1503, Dec. 2016.
- [63] B. Feng, K. Liu, T. Liu, J. Jiang, Y. Du, “Improving OFDR spatial resolution by reducing external clock sampling error”, *Optics Communications*, vol. 363, pp. 74 – 79. November 2015.
- [64] K. Iiyama and K. Yamaguchi, “Two-dimensional object profiling by FMCW optical sensing system using one-dimensional photodiode array,” *Int. Symp. Imaging, Sensing, Opt. Mem. Tech. Dig.* Pp. 139–40, 2017.
- [65] T. Hariyama, P. A. M. Sandborn, M. Watanbe, and M. C. Wu, “High accuracy range-sensing system based on FMCW using low-cost VCSEL”, *Opt. Express*, vol. 26, no.7, pp. 9285 – 9297, April 2018.
- [66] Song Zhang, “High Speed 3D shape measurement with structure light methods: A review”, *Opt. and Lasers in Engineering 106*, pp. 119 – 131, February 2018.
- [67] S. Moon, E. S. Choi, “VCSEL-based swept source for low-cost coherence tomography”, *Biomedical Opt. Express*, vol. 8, no. 2, pp. 1110 – 1121, January 2017.
- [68] S.H. Yun, G.J. Tearey, J.F. de Boer, N. Ifimia and B. E. Bouma, “High-speed optical frequency domain imaging”, *Opt. Express*, vol. 11, no. 22, pp. 2953 – 2963, November 2003.

APPENDIX

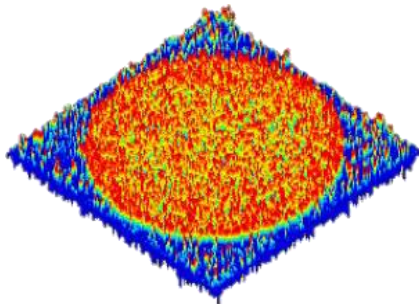
Object Profiling Result of a Japanese 100 YEN coin by FMCW Optical Ranging System using Symmetric Method are shown below.



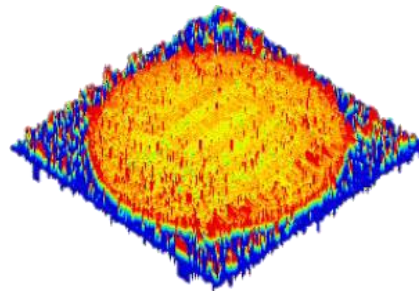
f_m 1 kHz, 6 mA, 700 points, 40.65 sec



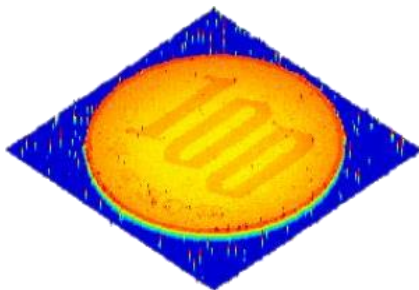
f_m 1 kHz, 6 mA, 300 points, 40.52 sec



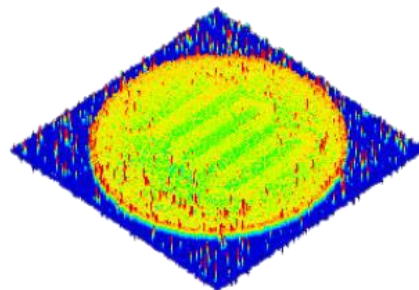
f_m 1 kHz, 4 mA, 700 points, 40.81 sec



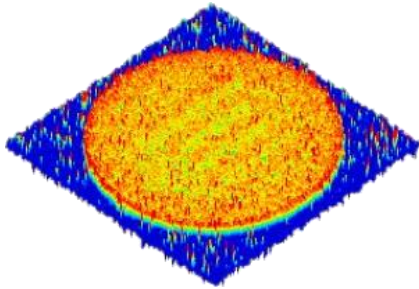
f_m 1 kHz, 4 mA, 300 points, 40.69 sec



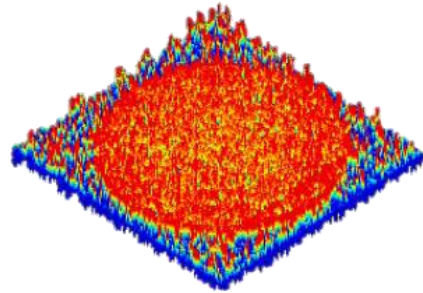
f_m 1.1 kHz, 6 mA, 1050 points, 37.02 sec



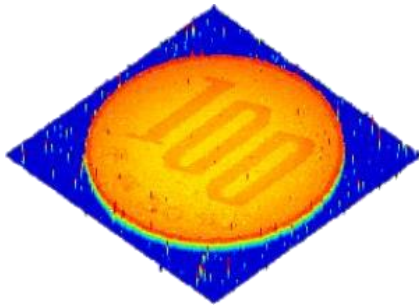
f_m 1.1 kHz, 6 mA, 300 points, 36.96 sec



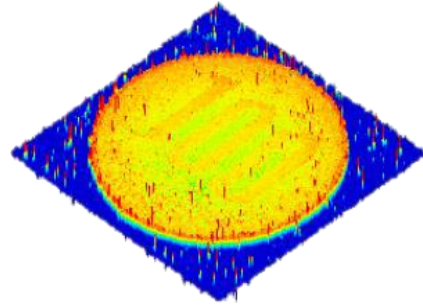
f_m 1.1 kHz, 4 mA, 650 points, 37.22 sec



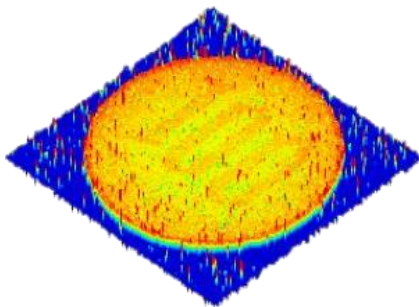
f_m 1.1 kHz, 4 mA, 300 points, 37.04 sec



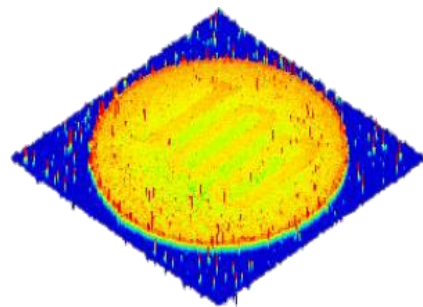
f_m 1.2 kHz, 6 mA, 1050 points, 33.98 sec



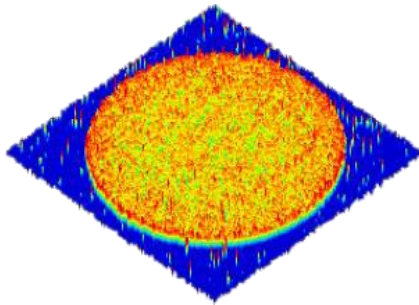
f_m 1.2 kHz, 6 mA, 300 points, 34.00 sec



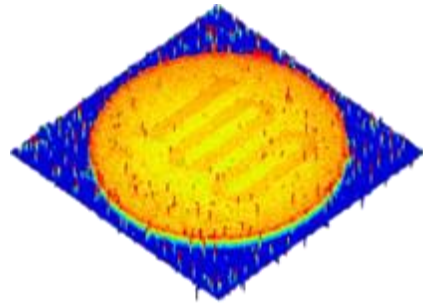
f_m 1.2 kHz, 4 mA, 650 points, 34.34 sec



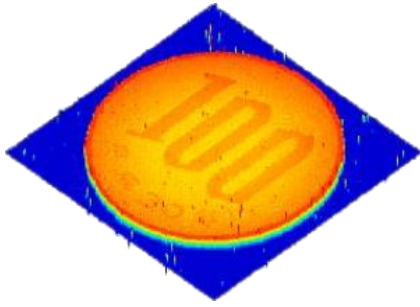
f_m 1.2 kHz, 6 mA, 300 points, 34.00 sec



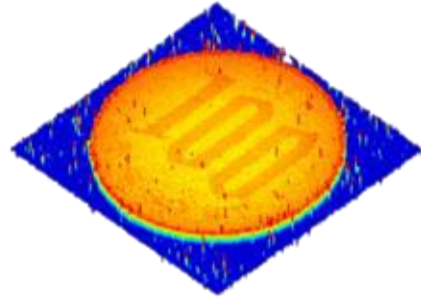
f_m 1.3 kHz, 4 mA, 1400 points, 67.10 sec



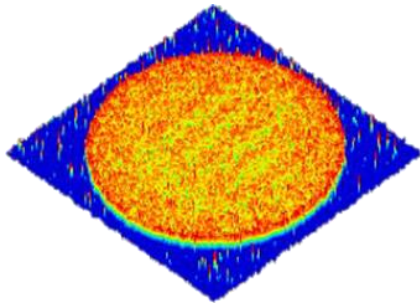
f_m 1.3kHz, 4 mA, 650 points, 31.33 sec



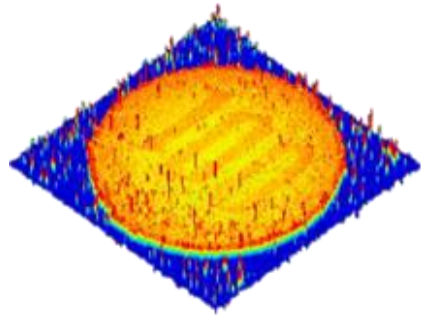
f_m 1.3 kHz, 6 mA, 1050 points, 31.43 sec



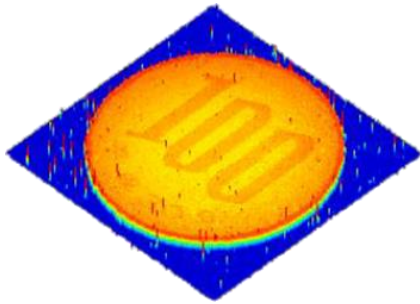
f_m 1.3kHz, 6 mA, 500 points, 31.47 sec



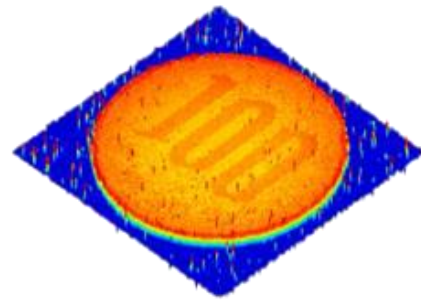
f_m 1.4 kHz, 4 mA, 1400 points, 61.10 sec



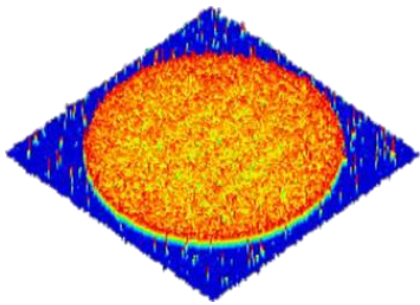
f_m 1.4 kHz, 4 mA, 300 points, 29.14 sec



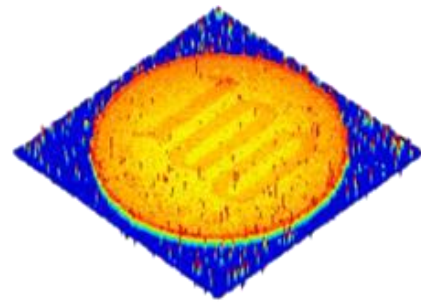
f_m 1.4 kHz, 6 mA, 1050 points, 30.67 sec



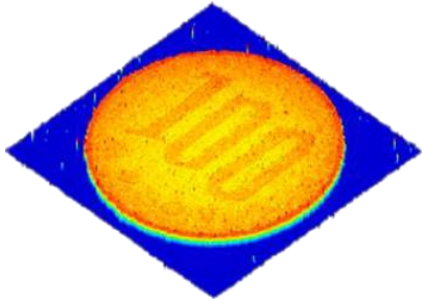
f_m 1.4 kHz 6 mA, 500 points, 29.30 sec



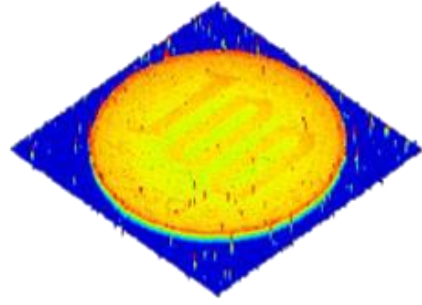
f_m 1.5 kHz, 4 mA, 1400 points, 54.21 sec



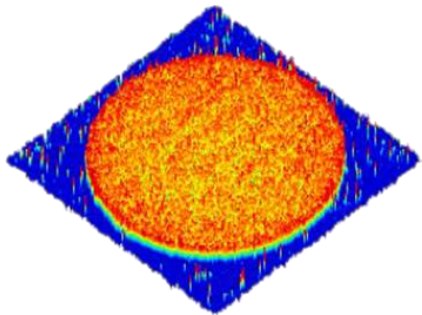
f_m 1.5 kHz 4mA, 650 points, 28.68 sec



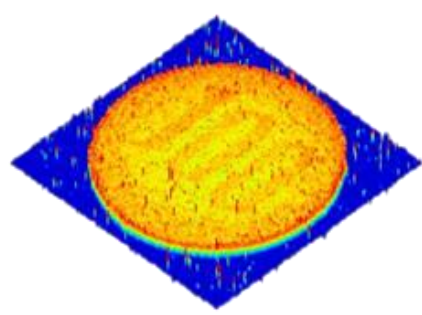
f_m 1.5 kHz, 6 mA, 1050 points, 28.98 sec



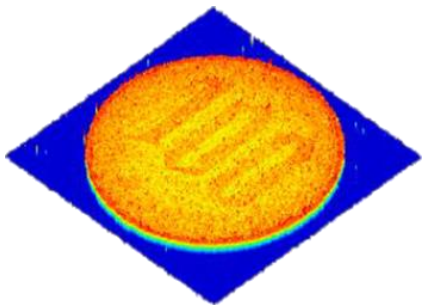
f_m 1.5 kHz, 6 mA, 500 points, 27.30 sec



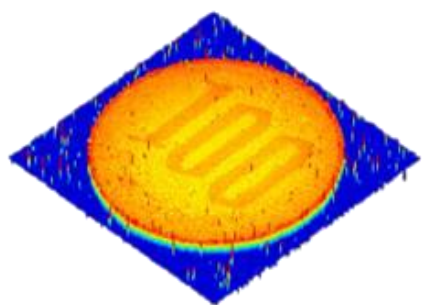
f_m 1.6 kHz, 4 mA, 1400 points, 50.86 sec



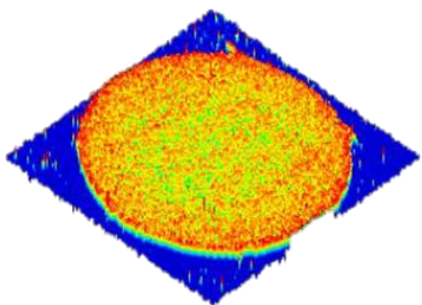
f_m 1.6 kHz, 4 mA, 650 points, 27.17 sec



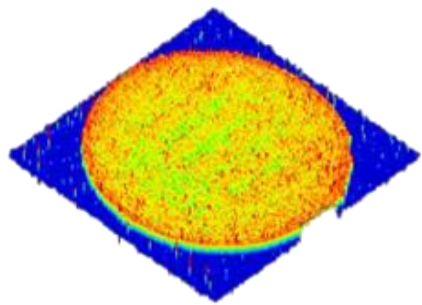
f_m 1.6 kHz, 6 mA, 1050 points, 27.47 sec



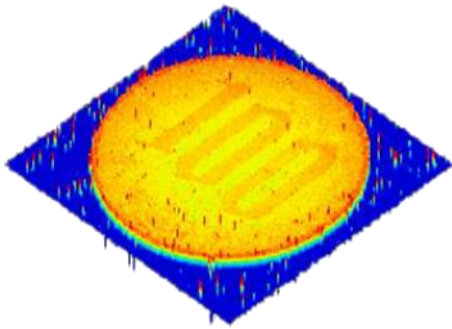
f_m 1.6 kHz, 6 mA, 500 points, 25.70 sec



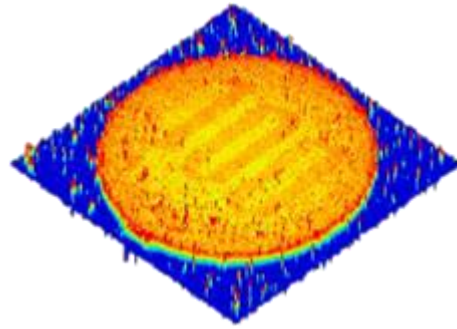
f_m 1.7 kHz, 4 mA, 1400 points, 47.88 sec



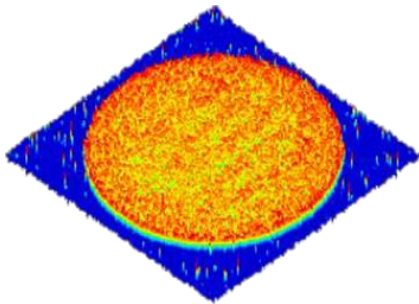
f_m 1.7 kHz, 4 mA, 650 points, 25.81 sec



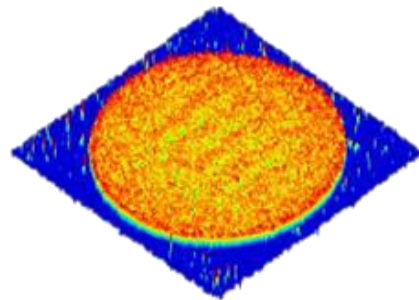
f_m 1.7 kHz, 6 mA, 500 points, 24.07 sec



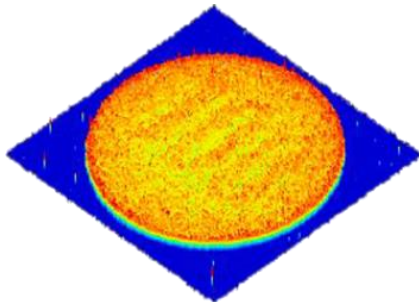
f_m 1.7 kHz, 6 mA, 300 points, 24.15 sec



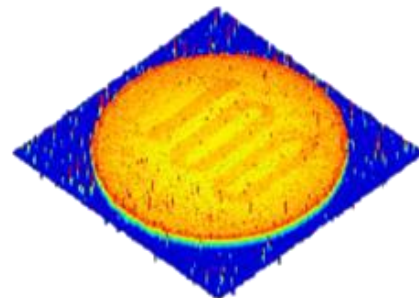
f_m 1.8 kHz, 4 mA, 1400 points, 45.257 sec



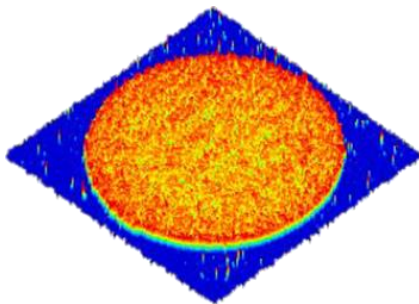
f_m 1.8 kHz, 4 mA, 650 points, 24.71 sec



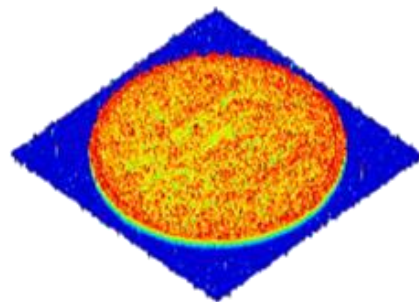
f_m 1.8 kHz, 6 mA, 1050 points, 25.25 sec



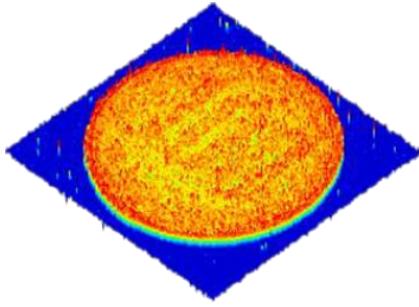
f_m 1.8 kHz, 6 mA, 500 points, 23.02 sec



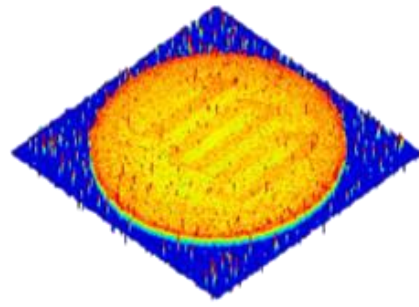
f_m 1.9 kHz, 4 mA, 1400 points, 42.79 sec



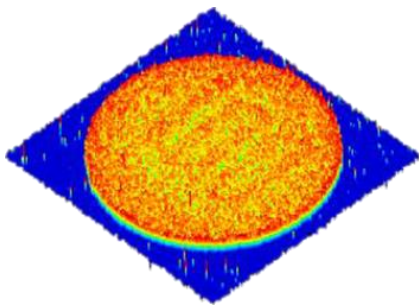
f_m 1.9 kHz, 4 mA, 650 points, 22.59 sec



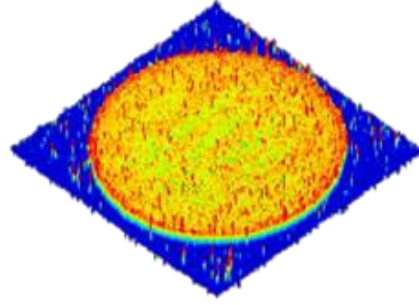
f_m 1.9 kHz, 6 mA, 1050 points, 25.1 sec



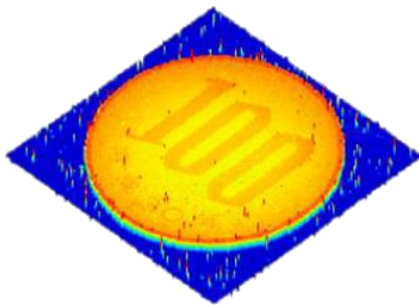
f_m 1.9 kHz, 6 mA, 500 points, 21.48 sec



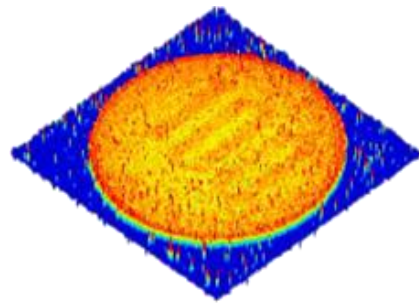
f_m 2.0 kHz, 4 mA, 1400 points, 40.72 sec



f_m 2.0 kHz, 4 mA, 300 points, 20.70 sec



f_m 2.0 kHz, 6mA, 1100 points, 40.69 sec



f_m 2.0 kHz, 6mA, 550 points, 21.32 sec